1 OF 1
AD A
107 985

END
DATE
FILMED
T -82
DTIC
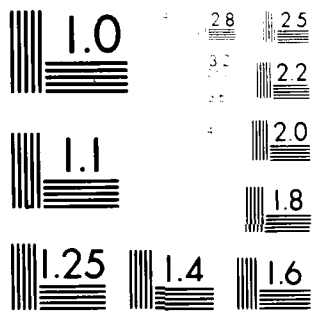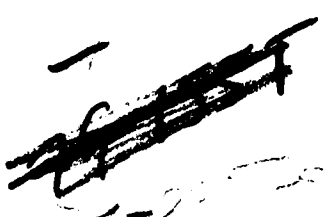
MICROCOPY RESOLUTION TEST CHART

SECURITY CLASSIFICATION OF THIS PAGE (When Data Entered)

REPORT DOCUMENTATION PAGE		READ INSTRUCTIONS BEFORE COMPLETING FORM
1. REPORT NUMBER 79-287T-S	2 GOVT ACCESSION NO. AD-A107985	3 RECIPIENT'S CATALOG NUMBER
4. TITLE (and Subtitle) Real-Time Forecasting of Echo-Centroid Motion		5 TYPE OF REPORT & PERIOD COVERED THESIS/DISSERTATION
		6 PERFORMING ORG. REPORT NUMBER
7. AUTHOR(s) Douglas Edward Forsyth		8 CONTRACT OR GRANT NUMBER(s)
9. PERFORMING ORGANIZATION NAME AND ADDRESS AFIT STUDENT AT: Univ of Oklahoma		10 PROGRAM ELEMENT, PROJECT, TASK AREA & WORK UNIT NUMBERS
11. CONTROLLING OFFICE NAME AND ADDRESS AFIT/NR WPAFB OH 45433		12 REPORT DATE 1979
		13. NUMBER OF PAGES 79
14. MONITORING AGENCY NAME & ADDRESS(if different from Controlling Office)		15. SECURITY CLASS. (of this report) UNCLASS
		15a. DECLASSIFICATION/DOWNGRADING SCHEDULE

LEVEL

16. DISTRIBUTION STATEMENT (of this Report)

APPROVED FOR PUBLIC RELEASE; DISTRIBUTION UNLIMITED

DTIC
ELECTE
DEC 1 1981
S D
H

17. DISTRIBUTION STATEMENT (of the abstract entered in Block 20, if different from Report)

23 NOV 1981

18. SUPPLEMENTARY NOTES

APPROVED FOR PUBLIC RELEASE: IAW AFR 190-17

FREDRIC C. LYNCH, Major USAF
Director of Public Affairs
Air Force Institute of Technology (ATC)
Wright-Patterson AFB, OH 45433

19. KEY WORDS (Continue on reverse side if necessary and identify by block number)

20. ABSTRACT (Continue on reverse side if necessary and identify by block number)

ATTACHED

"Original contains color
plates: All DTIC reproduct-
ions will be in black and
white"

DD FORM 1473 EDITION OF 1 NOV 65 IS OBSOLETE
1 JAN 73

SECURITY CLASSIFICATION OF THIS PAGE (When Data Entered)

81 11 30 014

THE UNIVERSITY OF OKLAHOMA

GRADUATE COLLEGE

REAL-TIME FORECASTING OF

ECHO-CENTROID MOTION

A THESIS

SUBMITTED TO THE GRADUATE FACULTY

in partial fulfillment of the requirements for the

degree of

MASTER OF SCIENCE

IN METEOROLOGY

By

DOUGLAS EDWARD FORSYTH

Norman, Oklahoma

1979

81 11 30

REAL-TIME FORECASTING OF

ECHO-CENTROID MOTION

A THESIS

APPROVED FOR THE SCHOOL OF METEOROLOGY

By

ABSTRACT

A program for real-time forecasting of echo-centroid
motions has been developed. The key to this development is
an algorithm for correlating previous with current storm-
centroid positions. The program was tested operationally
during the 1978 Joint Doppler Operational Project (JDOP) con-
ducted at the National Severe Storms Laboratory in Norman,
Oklahoma by the Air Force Geophysics Laboratory, the National
Severe Storms Laboratory and the Federal Aviation Administra-
tion. Program output was evaluated in both real time and
during post analysis. The sensitivity of the program to the
reflectivity threshold and correlation parameter was also
examined. Three different storm days were used during post
analysis to obtain quantitative results concerning forecast
accuracy.

Results of JDOP 1978 show that this approach to echo-
centroid forecasting is effective in providing forecasters
with a significant and timely assessment of storm-centroid
movement in an easily usable format. An examination of storm
tracks and forecasts reveals a mean forecast position error
of about 10 km for the three storms analyzed. However, for
more severe storms, the forecast error is smaller. For

example, in the storm producing the Marlow tornado on 5 April 1978, the mean 12-min forecast position error was 4.38 km with a standard deviation of 2.98 km. The system correctly predicted a direction of storm movement different from the National Weather Service forecast. This deviation was detected in sufficient time for a forecast revision. Because of this performance, the system was credited with saving the lives of a couple whose home was destroyed by one of the storm's tornadoes.

ACKNOWLEDGMENTS

TABLE OF CONTENTS

LIST OF FIGURES

LIST OF TABLES

LIST OF SYMBOLS AND ABBREVIATIONS

$\Delta\theta$	Distance between azimuths
Δr	Range element
φ	Antenna elevation angle
μsec	Microsecond
θ_j	Azimuth
A_x	Unbiased estimator of regression coefficient
A_y	Unbiased estimator of regression coefficient
AFGL	Air Force Geophysics Laboratory
ALPHA	Azimuth threshold
B_x	Unbiased estimator of regression coefficient
B_y	Unbiased estimator of regression coefficient
cm	Centimeter
CPM	Cards per minute
CPU	Central Processing Unit
CRT	Cathode Ray Tube
CST	Central Standard Time
dbZ	10 log Z
DCOR	Correlation parameter
DDI	Data Display Interface
deg	Degree
DMA	Direct Memory Access

ESELCH	Extended Selector Channel
FAA	Federal Aviation Administration
GCK	Garden City, Kansas
GRND	Ground clutter elimination criterion
HBR	Hobart, Oklahoma
IBM	International Business Machines
I/O	Input/Output
JDOP	Joint Doppler Operational Project
km	Kilometer
kW	Kilowatt
LBL	Liberal, Kansas
LLS	Linear least-squares
LPM	Lines per minute
LSU	Loader Storage Unit
LTS	Altus, Oklahoma
m	Meter
M_{AREA}	Z-weighted area
MAC	Memory Access Controller
MB	Megabyte
MHz	Megahertz
min	Minute
mm	Millimeter
NA	Azimuth location for storm segment
NRC	Number of range cells
NSSL	National Severe Storms Laboratory
OVLP	Range cell overlap threshold

PASLA	Programmable Asynchronous Serial Line Adapter
PPI	Plan Position Indicator
PPP	Pulse Pair Processor
PPRI	Pulse Pair Recorder Interface
PRF	Pulse Repetition Frequency
PVA	Positive Vorticity Advection
r_i	Range cell number
RHO	Range cell threshold
SCRM	Scan Converter-Refresh Memory
SRI	Stanford Research Institute
SWO	Sweetwater, Oklahoma
t	Time
T_d	Pulse width
t_ℓ	Latest time
TSD	Total distance error
TTY	Teletype
ULIM	Universal Logic Interface Module
$\bar{X}$	X-position of centroid
$\bar{X}_e$	Mean forecast error
X_f	Forecast position of centroid in X-direction
X_ℓ	Latest position of centroid in X-direction
$\bar{Y}$	Y-position of centroid
Y_f	Forecast position of centroid in Y-direction
Y_ℓ	Latest position of centroid in Y-direction
Z	Reflectivity
ZTH	Reflectivity threshold

1. INTRODUCTION

Within the last 20 years, there have been many attempts to obtain a fast and reliable method of predicting radar echo motion. One of the first applications of modern objective techniques to forecasting echo displacement was reported by Hilst and Russo (1960). These techniques relied on spatially correlating Plan Position Indicator (PPI) information to derive echo motion and speed. These techniques and others by Wilson (1966) and Blackmer and Duda (1972) provided a single speed and direction of motion for the whole radar scope. However, individual storms may have quite different motions. For example, when severe storms split, the left portion often travels faster then the mean wind and the right portion slower than the mean wind (Newton and Fankhauser, 1964). In 1970, Barclay and Wilk (1970) developed a technique to identify and track radar echoes from automatically digitized radar data. Their experiments showed that the use of higher threshold values for tracking caused erratic echo-centroid* motions. They also noted that the large echoes were more consistently tracked. To obtain a forecast position for the echo, they

---

*Refers to center of mass.

1

applied a linear least-squares algorithm to the centroid posi-
tions giving more weight to recent observations and to echoes
with higher reflectivity. Wilk and Gray (1970) later reported
that they had applied this basic system to forecasts ranging
from 15 to 60 min. They concluded that the optimum sampling
interval for a 60-min forecast was 45 min with a corresponding
forecast error of 10 n mi and a standard deviation of 10-15
n mi.

Blackmer, Duda, and Reboh (1973) refined Blackmer and
Duda's earlier model to use a pattern recognition technique
to isolate and track the radar echoes. This refined model is
the Stanford Research Institute (SRI) model. The SRI tech-
nique assigns the isolated echoes a significant weight depend-
ing on their size and intensity. A weight threshold is then
applied to determine those echoes to be tracked. If the cri-
terion is met, a window is placed around the echo. The windows
are the entities that are tracked. The extrapolation of future
echo positions are made by a weighted combination of the latest
observed window displacement and the previous forecast displace-
ment.

More recently, Elvander (1976) presented results of a
study where he compared the performance of three methods for
forecasting echo motion. The methods used were (1) an adapted
version of the Canadian technique [described by Austin and
Bellon (1974)] that utilizes the entire PPI to obtain dis-
placement vectors, (2) a linear least-squares (LLS) algorithm

for extrapolation of echo centroids* similar to that used by Wilk and Gray (echo centroids were obtained from the SRI model), and (3) the SRI model. Elvander concluded that the Canadian model was the best with the LLS method being the poorest.

The term "echo centroid" can be defined in several different ways. The two most common definitions refer to either the center of an area or the center of mass. In this study, an echo centroid will refer to the center of mass of an echo determined by the center of the Z (reflectivity) - weighted area (analogous to mass if Z were mass per unit area) of the echo.

The aim of this study is to develop a real-time echo-centroid forecast program. Although Elvander contended that there are better forecast techniques than the LLS method, these techniques result in a loss of the fine scale movement of the individual echoes. Also, they are not easily adapted for real-time use. On the other hand, the LLS method for forecasting echo-centroid movement is simple to develop and apply to real-time operations. This method also retains the fine scale movement of the individual echoes.

Boak, et al., (1977) developed a program for the Air Force Geophysics Laboratory (AFGL) to calculate echo centroids and display their locations along with the echo outline. This

---

*Elvander's paper did not state whether these were centers of area or mass.

work was used as a stepping stone for developing the correlation and forecast algorithms.

The term correlation is not used in a strict statistical sense. In this study, correlation refers to the mutual relation of a previous echo centroid to a current echo centroid. Thus, when a correlation occurs between the two centroid positions, the echoes associated with these centroids are considered to be the same echo.

The correlation algorithm is the key to all other work done in this study. Without an efficient and effective method of correlating past with present echo-centroid positions, real-time tracking and forecasting of these positions would be impossible. The simple approach applied here is an initial attempt to obtaining such a method.

The author's correlation algorithm and a forecast algorithm, similar to that used by Zittel (1976), were added to the Boak, et al., original program. These were combined with improvements in the color display presentations to obtain the real-time echo-centroid forecast program.

The final program was tested in an operational environment during the 1978 Joint Doppler Operational Project (JDOP) conducted at the National Severe Storms Laboratory (NSSL) in Norman, Oklahoma, by the Air Force Geophysics Labortory, the National Severe Storms Laboratory, and the Federal Aviation Administration (FAA). System usefulness was evaluated during

the real-time operation and also through post analysis of
three different storm cases. It is hoped that the results
presented here will lead to more improvements in the area of
real-time analysis of Doppler radar data.

2. SYSTEM DESIGN

a. Hardware Description

The hardware needed to operate a real-time echo-centroid forecasting system includes a radar with digital output of logarithmic, range-corrected reflectivity data, encoders to prepare the data for processing by a minicomputer, and a scan converter/refresh memory and colored Cathode Ray Tube (CRT) for displaying the computer output.

In particular, this study utilized the antenna and transmitter from the National Severe Storms Laboratory in Norman, Oklahoma. The 10 cm Doppler radar's characteristics are listed in Table 1. The receiver and all other equipment were furnished by the Air Force Geophysics Laboratory. The receiver characteristics are contained in Table 2. The system is illustrated in block diagram form in Fig. 1.

The receiver is called a Pulse Pair Processor (PPP) and was developed by Raytheon for the Air Force Geophysics Laboratory to reduce the vast quantities of data to a form suitable for real-time operation and archiving. "In particular, the PPP develops logarithmic reflectivity, mean Doppler velocity, and Doppler spectrum variance for 256, 512, 768, or 1024 range cells of 0.5, 1.0, or 2.0 μsec (75, 150, or 300 m) with batch type

integration of between 1 and 1024 radar pulse periods. The amount of information generated in a single 360 degree azimuth scan, typically less than a minute in duration, approaches 10 million bits with a one-degree-beam-width antenna." (Boak, et al., 1977). The parameters used in this study were 768 range cells of 150 m with a batch integration of 128 radar pulse widths.

From the PPP, the data (reflectivity, velocity, and variance) travels to the encoder/decoder where it is put in a form usable by the FR 2000A wideband instrumentation recorder for archiving and by the 7/32 Interdata minicomputer. The data also travels to the Scan Converter-Refresh Memory (SCRM) system to be displayed on the three color CRT's.

The computer system is illustrated in Fig. 2. It consists of 192K bytes of memory and has 6 digit single precision accuracy. Both low and medium speed peripherals communicate with the Central Processing Unit (CPU) through the input/output (I/O) multiplexer bus[*]. The SCRM is connected to the computer via an interface constructed on a Universal Logic Interface Module (ULIM). This permits use of one or more of the SCRM's bit image memory/color display channels for plotting outputs in color graphic form.

The magnetic disc bulk storage unit has a five megabyte

---

*Multiplexer bus is a channel or line that can carry several units of information simultaneously from one portion of the computer to another.

two-surface fixed platter and a five megabyte removable cart-
ridge. The disc contains 408 4-track cylinders with an aq-
uisition time of 60 milliseconds or less. The disc communi-
cates with the CPU via an Extended SELector CHannel (ESELCH)
because of the transfer rate involved.

Another ESELCH supports the major radar input port:
the Pulse Pair Recorder Interface (PPRI). The PPRI prepares
the data for use by the computer and transfers it to the CPU
via Direct Memory Access (DMA) through the 16-bit wide ESELCH.
The data are transferred at 70K bytes sec^{-1}.

b.   Software Configuration

The original Raytheon software was used as a building
block for the real-time echo-centroid forecasting program.
This software is summarized below. For a detailed description,
consult the final R & D Equipment Information Report-Tracking
and Significance Estimator by Boak, et al. (1977). A system
timing diagram (Fig. 3) of the original software gives an over-
all picture of the data processing.

1)   Data Acquisition

Data acquisition begins with the transfer of data from
the PPP to the system disc. As the radar scans in azimuth for
the requested number of degrees, the radar video signals pro-
cessed in the PPP, enter the PPP encoder and are combined with
ancillary data. From the encoder, the data are processed by
the PPRI and placed on the disc azimuth by azimuth.

Data acquisition can be done in either of two modes: sector scan or PPI. In both cases, data are stored only when the elevation angle of the radar is within acceptable limits. In the PPI mode, the program begins collection at the first azimuth that the elevation angle is acceptable and terminates when the azimuth is passed again.

2) Storm*-Centroid Calculations

The storm-centroid calculations take place in three phases: 1) Range processing, 2) Azimuthal processing and 3) Area and center processing.

During the data acquisition phase, the beginning and end points of the meaningful data segments are stored. A segment is considered meaningful if its power Z is above the selectable threshold ZTH for more than RHO range cells in radial extent. Three summations are made during this phase of the processing:

$$\sum_{i=1}^{NRC} r_i \, \Delta r$$

$$\sum_{i=1}^{NRC} Z(r_i, \theta_j) \Delta r \, r_i$$

$$\sum_{i=1}^{NRC} Z(r_i, \theta_j) r_i^2 \, \Delta r$$

where the summations are over the range cells that were

---

*Storm refers to an area within an echo that has met the criteria of the program.

considered meaningful. The range cell number (r_i) varies from one to NRC, where NRC (total number of range cells) is determined by the Pulse Repetition Frequency (PRF). θ_j is the current azimuth being processed. The range element ($\Delta r = 150\ T_d$ cos φ m sec^{-1}) represents the flat earth ground range of one radar cell where φ is the antenna elevation angle and T_d is either 0.5, 1.0, or 2.0 μsec depending on the pulse width. The pulse width was 1.0 μsec for this study. By controlling the initial range cell number, the ground clutter can be eliminated from the data. If more than 11 different segments are obtained in one azimuth, only the 11 largest segments are retained for azimuthal processing.

The second phase is the azimuthal processing. The beginning and end points obtained in the previous phase are now checked for azimuthal extent. The criterion ALPHA is established for the minimum number of adjacent azimuths to be considered a storm. ALPHA is determined approximately by dividing RHO by the range cell number to keep the azimuthal and range criteria approximately equal. The OVLP criterion determines the minimum number of cells that must overlap for the segment to be considered part of the same storm.

If the ALPHA and OVLP criteria are met, the combined segments are accepted and assigned a storm number. Fig. 4 illustrates two different examples of the above criteria. Example one would be accepted as the same storm segment,

while example two would be considered as two separate storm segments.

In the last phase, the following summations are computed:

$$M_{Area} = \sum_{j=1}^{NA} \sum_{i=1}^{NRC} Z(r_i, \theta_j) r_i \, \Delta r \Delta \theta$$

$$Sum1 = \sum_{j=1}^{NA} \sum_{i=1}^{NRC} r_i^2 \sin \theta_j \, Z(r_i, \theta_j) \Delta r \Delta \theta$$

$$Sum2 = \sum_{j=1}^{NA} \sum_{i=1}^{NRC} r_i^2 \cos \theta_j \, Z(r_i, \theta_j) \Delta r \Delta \theta$$

where M_{Area} is the Z-weighted area (analogous to mass if Z were mass per unit area), NA is the azimuth location for that storm segment and $\Delta \theta$ is the distance between adjacent azimuths.

M_{Area} is used to determine the 12 largest storms to be saved for further processing. The final step in this phase is to determine the Z-weighted centroid positions $(\bar{X}, \bar{Y})$ for each storm.

$$\bar{X} = \frac{Sum1}{M_{Area}}$$

$$\bar{Y} = \frac{Sum2}{M_{Area}}$$

Centroid characteristics such as maximum reflectivity, maximum velocity, and maximum variance are then stored for later use.

3) <u>Data Display</u>

The original data were plotted as shown in Fig. 5. The

scaling and origin location were taken from the SCRM when in use for direct display of PPP data. Thus, the data were displayed with the same scaling and origin location as the reflectivity and velocity data. Range markers appeared as red concentric circles centered about the radar origin. A "+" indicated the centroid position $(\bar{X}, \bar{Y})$. The actual storm outline was also plotted. The centroid positions obtained for previous times were plotted for up to 24 past time sequences in different colors for each time. The characteristics [range, azimuth, area, maximum reflectivity, maximum velocity, maximum velocity standard deviation and mass (Z-weighted area)] could be obtained for all past storms by executing a separate program called DUMP.

c. Software Modifications and Additions

Several modifications and additions to the original software were required in order to develop a real-time echo-centroid forecasting program. This involved modifying the data acquisition process, developing the correlation and forecast algorithms and improving the data displays.

1) Data Acquisition

The first modification involved obtaining compatibility between the software and the National Severe Storms Laboratory's Doppler radar. The original program was designed to accept 448 radials of data. The Norman Doppler radar rotates at a much slower speed than the Air Force Geophysics Laboratory's radar. This slower rotational rate resulted in 600

radials of data from the PPP when 128 spectral sweeps were integrated. In order to minimize the modifications, approximately every other radial was used in the program. This provided a resolution between azimuths of either 0.6 or 1.2 degrees. Although the program operated satisfactorily, the most desirable resolution would have been 0.81 degrees (half-power-beam-width of the radar).

The second modification refined the elevation angle limits used for tracking. As noted previously, data acquisition is dependent upon the elevation angle whose resolution is in whole degrees. Thus, the program gathered data when the elevation angle was between 0.0 and 0.9 degrees. In order to operate with a tilt sequence (i.e., 0.2, 0.6, 1.0, 1.6 degrees, etc.), the resolution of the elevation angle limits were modified to accept tenths of degrees.

2) Correlation Algorithm

The correlation algorithm was developed to correlate previous with current centroid positions. The algorithm allowed for a maximum movement of the storm centroid in both the X and Y direction based on the interval between acquisition times. The initial guess of this correlation parameter (DCOR) was one $km\ min^{-1}$. Thus, if the acquisition time interval was six min, the program would correlate the present centroid position with the previous centroid position(s) if they were within six km in either the X or Y direction. Based on initial testing, one $km\ min^{-1}$ proved to be too small.

Because centroid movement was larger than anticipated, very few echoes could be correlated. Since DCOR was an integer value, it was increased to two km min^{-1} for real-time operation. A discussion of the program sensitivity to a given value for DCOR is presented later.

The storms are rank ordered according to Z-weighted area from largest to smallest. Normally, the storm's Z-weighted area changes at a slow enough rate so that the largest storms tend to remain the largest storms during the time between data acquisitions. The algorithm processes the largest Z-weighted area storm first and attempts to relate it to the previous largest storm. This increases the probability that the correct correlation will be made.

This algorithm also handles the merging and splitting of storms. For splitting, the centroid position associated with the largest Z-weighted area is correlated to the past position, while the smaller one(s) are considered as new storm(s). If the smaller one(s) remain split and become correlated during the next acquisition, they are then tracked. For the storms that have merged, the new centroid's position is correlated with the larger of the previous storm centroid positions and the track for the smaller one(s) are ignored. The handling of storm merging/splitting is based on evidence that the larger storms are stronger storms (Bjerkaas, 1977). The stronger storms are the most potentially dangerous and thus are given priority in this algorithm.

To illustrate how the correlation algorithm works,

consider the following example. Initially, two storms, A_1 and B_1, have their centroids located at (X = 2, Y = 19) and (X = 10, Y = 5), respectively, (Fig. 6). During the next 6 min, storm B_1 traveled to location (X = 17, Y = 13), while storm A_1 dissipated. Processing of the current centroid B_2 begins with a search in both the X and Y directions for any previous centroid positions that are within a 24 km square box centered on the current centroid position. Storm A_1 had the largest Z-weighted area 6 min earlier and is therefore checked first. It does not meet the criterion and no correlation is made. However, storm B_1 was the next largest storm checked and it does meet the criterion. Therefore, storm B_1's centroid position is correlated to storm B_2's centroid position. This relationship is recorded in a correlation table and the processing of storm B_2 terminates. If storm A_1 had met the criterion, its centroid position would have been correlated with storm B_2's and storm B_1's centroid position (even though it met the criterion) would not have been correlated. Thus, only one correlation (the centroid position associated with the largest Z-weighted area) is allowed per storm.

An example of the correlation table is shown in Table 3. The rows are rank ordered according to Z-weighted area; the columns represent the acquisition time (up to 24 different values).

The table numbers are indices used to locate data in other tables associated with the related storms. If data

have been accumulated for more than 24 times, the oldest data
are dropped from the table. The indices are positive if the
current storm is related to the previous storm and negative
if it is not. For the initial time, the indices are all
negative.

For the example above, the correlation table is shown
in Table 3. As mentioned earlier, the storms are rank ordered
according to Z-weighted area from largest to smallest. There-
fore, at Time 1 (1200 CST for this example), A_1 is Storm 1
and B_1 is Storm 2. At Time 2, B_2 is Storm 1. Because B_2's
centroid position was correlated to B_1's centroid position,
this relationship was noted in the table by making the -2
index (located at Storm 2, Time 1) positive and placing it
in the proper table position (Storm 1, Time 2). At Time 3
(not shown in Fig. 6), the second largest storm was related
to B_2 as noted by the index 2 for Storm 2 at Time 3. Thus,
the related storms can be followed through time by use of the
indices. Storm A_1 on the other hand, does not exist at Time 2
and is therefore denoted by the index -1. The index -1 would
also be used if storm A_1 still existed at Time 2, but was not
related to any other storm.

3) Forecast Algorithm

The forecast algorithm uses the correlated storm-cen-
troid positions to compute a forecast. By performing a least-
squares fit on these positions, 12- and 24-min forecast posi-
tions are obtained. The algorithm consists of computing the

sum of squares (Zittel, 1976) and obtaining the coefficients for the following equations:

$$X_f = A_x t + B_x$$

$$Y_f = A_y t + B_y$$

where

$$A_x = \frac{N\Sigma X \ t - \Sigma X \Sigma t}{N\Sigma t^2 - (\Sigma t)^2}$$

$$A_y = \frac{N\Sigma Y \ t - \Sigma Y \Sigma t}{N\Sigma t^2 - (\Sigma t)^2}$$

and t is the actual forecast time in min.

$$B_x = X_\ell - A_x t_\ell$$

$$B_y = Y_\ell - A_y t_\ell$$

Where t_ℓ, X_ℓ, and Y_ℓ are the centroid's latest position in time and space.

Unlike Zittel's method, the forecast algorithm uses all observations with a weighting factor of one. Thus, an increase in the number of observations used to make the forecast reduces the influence of the latest observation. This results in a forecast that is less and less influenced by the individual centroid shifts.[*] This method appears reasonable considering the larger most sustained storms tend to travel in a straight line after initial movement is established.

_____

[*]Centroid shift is the apparent storm movement due to a change in the centroid position by other then the storm motion.

This straight line movement is the basis for using a linear least-squares fit rather than a higher order polynomial fit to the centroid positions. The linear least-squares method is also easier to accomplish and requires less computer time and storage. An illustration of the forecast algorithm is presented below.

To obtain a forecast for a storm-centroid position, the storm's index is obtained from the correlation table. If the index is positive, it is used to obtain the summations for use in the least-squares equations. Again looking at the correlation table (Table 3), at Time 3, the program makes a forecast for Storm 2 based on three observations, while the forecast for Storm 1 (Index 1) is based on two observations. Once the coefficients of the least-squares equations are obtained, they are stored for later use in computing the forecast errors.

Although A_x and A_y are computed as stated above for real-time operation, a more reliable calculation can be obtained (considering the Interdata 7/32 only contains 6 digit single precision accuracy) by using the long method instead of the sum of squares. Thus, A_x and A_y are computed as follows for post analysis:

$$A_x = \frac{\Sigma(X_i - \bar{X})(t_i - \bar{t})}{\Sigma(t_i - \bar{t})^2}$$

$$A_y = \frac{\Sigma(Y_i - \bar{Y})(t_i - \bar{t})}{\Sigma(t_i - \bar{t})^2} \ .$$

The 12- and 24-min values for forecasts are arbitrary and based on an estimated acquisition of data every six min. During real-time operations, the time between acquisitions varied from 6 to 13 min. This time interval was a function of the number of elevation angles being used. Based on the initial estimate, the forecast and actual positions are easily compared to determine the relative value of this method.

Forecast errors were computed in real time. Included were a speed error, direction error, and a total error based on the last forecast position.

The speed and direction errors were calculated by using the past forecast coefficients that most closely corresponded to those at the current time minus 12 or 24 min. These forecast coefficients were then used to obtain a forecast position for the current time. The speed error was obtained as shown in Fig. 7. The distance (CO) from the original centroid position (centroid used to make the original forecast) to the new forecast position was subtracted from the distance (BO) from the current centroid position to the original centroid position. This resulted in a length error that was divided by the time difference (current time minus original time) to obtain a speed error. The direction error was obtained by subtracting the direction the storm centroid actually moved from the forecasted movement (Fig. 7). This error was displayed in degrees per minute.

The total error for the last forecast is obtained as

shown in Fig. 8. A forecast position (C) is computed for the current time. The current position (A) is then subtracted from the forecast position (C) to obtain a total error in the forecast since the last acquisition time. Thus, forecasters can obtain a real-time evaluation of the past performance of the algorithm. A similar total error is used in post analysis and is discussed later.

4) Data Display

Data displays are an important facet in any operation. In order for the data to be useful, it must be presented to the forecaster in the clearest way. Interaction with the computer must be minimized as much as possible. Therefore, several improvements were made to the original display.

The storm-centroid tracks were now available for display based on the correlation algorithm. The SCRM contains no hardware for the generation of graphics. Therefore, a software routine for plotting on the CRT was developed. This routine allowed for plotting straight lines between the past and current centroid positions; these lines showed the storm-centroid track. The 12- and 24-min forecast centroid movements and an overlay of the state of Oklahoma were also plotted using this routine.

In order to quickly identify the characteristics associated with the different storm centroids, a method of annotating the display was developed. A character generator providing 64 characters was created. This allowed for a display

of the times associated with the past, current, and forecast positions along with the storm-centroid number. An example is shown in Fig. 9. The current centroid positions are labeled with a hexadecimal number from 1-C. The track segments are color coded and are related to the times in the legend; i.e., they are displayed in the same color. The 12- and 24-min forecast positions, denoted by a "+", are also color coded and are related to the times in the legend preceded by an F.

The characteristic list is shown in Fig. 10. Each storm is assigned a hexadecimal number. This number is used as the area number in the characteristic list and as the storm number on the CRT display. The characteristic list was expanded to include the current speed of the centroid and direction of movement, and for each forecast, the forecast position of the centroid (range and azimuth), the direction and speed error, and the total error (TSD) since the last forecast. The date, time and parameter values are also listed.

3. REAL-TIME OPERATION

The first real-time operation of this system occurred during the 1978 Joint Doppler Operational Project conducted at the National Severe Storms Laboratory in Norman, Oklahoma. JDOP's goal was the evaluation of the Doppler radar for real-time operations and the use of different color displays and data presentations. Thus, the echo-centroid forecasting system provided real-time information that was given to the United States Air Force Base Weather Stations and to the National Weather Service (NWS) for use in preparing warnings.

During real-time operation, a ZTH threshold of 30 dbZ* was used with RHO equal to 14 range cells and OVLP equal to 5 range cells. The antenna scanned in the PPI mode and was normally elevated in 6 distinct steps from 0.2 degrees elevation to 6.0 degrees elevation (i.e., 0.2, 0.6, 1.0, 2.0, 4.5, and 6.0 degrees). The echo tracking and forecasting routine obtained the data from the lowest elevation angle (normally 0.2 degrees). Thus, with six elevations to be scanned, a 12- and 24-min forecast was generated approximately once every 6 min during the JDOP operation.

---

*dbZ is defined as $dbZ = 10 \log Z$, where Z is equivalent reflectivity factor in $mm^6 \ m^{-3}$.

Speed and direction of movement were not only used for the issuance of warnings, but were used as input parameters to the NSSL displays. The input of this information allowed NSSL to automatically remove storm motion from its velocity displays and thus present a clearer picture of the actual storm velocities.

4.   DATA AND METHODOLOGY

Although an evaluation of this system was continually performed during the real-time operation, data on several storm days were collected for post analysis.

a.   Case Studies

Three separate days were chosen for post analysis. Tornadoes occurred on two of the days; on the other day slow moving storms that produced heavy rain were observed. The synoptic situations presented below are courtesy of John Weaver of NSSL.

1)   Case 1 - 5 April 1978

The synoptic situation was favorable for severe weather. The 0600 CST 500-mb analysis (in combination with satellite data) revealed a rather intense shortwave centered in southeastern Utah. The numerical guidance forecasted this system to move due eastward toward Liberal, Kansas (LBL) during the day. Positive Vorticity Advection (PVA) was predicted to occur around noon in western portions of Kansas and Texas. At 0900 CST, the surface analysis showed a strengthening dry boundary from Garden City, Kansas (GCK) southward through the eastern Texas panhandle. Lifted indices throughout the region were between -5 and -8. The vertical wind shear was strong.

Thunderstorms began forming along the dry line in western Kansas about 1330 CST. Convective towers along the boundary in western Oklahoma formed, then eroded, for most of the afternoon. They began to intensify rapidly at about 1700 CST. A list of the severe activity is given in Table 4. The Marlow, Oklahoma tornado occurred at 2024 CST and was F2 intensity according to the Fujita scale (Fig. 11). Three other tornadoes also occurred on this day. Data were collected between 2023 and 2247 CST for post analysis.

2) Case 2 - 9 April 1978

The synoptic situation on this day was not as favorable for tornadic activity. The morning synoptic data indicated a developing severe thunderstorm situation in western Oklahoma and central Texas. Composite analysis revealed a dry line moving into a very unstable air mass in western Oklahoma. This region was being overrun from the south-southwest by an 850-mb moist tongue that was, in turn, beneath a sharply diffluent zone at 500 mb. A moderately strong wave approaching this area from the southwest was identified on satellite photos. Working against tornado potential were weak meridional winds and advection of moisture at 700 mb.

At 1230 CST, a line of activity began along the western Oklahoma border and began moving eastward. The echoes to the North were very slow moving storms and caused local flooding in that area, while the storms along the southern end moved fairly rapidly and contained a mesocyclone. Large hail and

strong winds occurred during the period of data collection
(1558 to 1838 CST). A list of the severe activity is given
in Table 5.

3) Case 3 - 30 April 1978

The synoptic situation on this day was again favorable
for development of tornadic storms. The morning surface anal-
ysis revealed an organized low in southwestern Oklahoma with
a warm front extending from the low on a line from Altus, Okla-
homa (LTS) to Hobart, Oklahoma (HBR) to Sweetwater, Oklahoma
(SWO). A dry line was moving into central Texas. An upper
shortwave, combined with a very unstable air mass (lifted in-
dex at Oklahoma City of -9) was expected to trigger severe
storms along both the warm front and dry line by mid-afternoon.
Stronger upper air winds at Midland and Stephenville, Texas
indicated better tornado potential south of the Red River. At
1500 CST, severe storm chasers reported towering cumulus grow-
ing near Lawton, Oklahoma. The cumulus were shearing dramatic-
ally with height.

Several severe weather events (Table 6) occurred in Okla-
homa including a major tornadic storm that produced nine sepa-
rate tornado damage paths as it moved from El Reno to north-
western Oklahoma City (Fig. 12). The intensity of the torna-
does ranged from F3 to F4. Data for post analysis was col-
lected from 1656 to 1901 CST. The tornadoes occurred between
1740 and 1830 CST.

b.   Data Types

For each case listed above, data were obtained using several different ZTH threshold settings (25, 30, 35, and 40 dbZ). These data were used for testing the sensitivity of the system to various tracking thresholds.

From these data, a simulated data set was obtained by converting the original range and azimuth information back into rectangular coordinates. The echo-centroid forecasting program (adapted to the IBM 370/158) was then used to test the forecast sensitivity to different correlation parameter (DCOR) values.

The simulated data set contains an induced error. The real-time data set had X and Y's that were converted to integer values of range and azimuth for display. These integer values were then converted back into rectangular coordinates for post analysis. The error is the difference between the real-time and post analysis values for X and Y. The average error is less than 0.5 km for the X and Y position. Thus, the effect of the errors on the results of this study are considered minimal. These "bogus" data are also used to compare the different ZTH thresholds for storms larger than 4000 dbZ km^2.

c.   Error Analysis

The forecast accuracy was determined by comparing the forecast position to the actual position. The forecast position was computed by taking the actual position, subtracting

12 or 24 min from the current time to find the coefficients of the least-squares equation, and computing the forecast position based on these coefficients. This position (C) was then compared to the actual position (B) to obtain a distance error (BC) for the forecast (Fig. 13).

The speed and direction errors were also considered for use in comparing the forecasts; however, the distance errors were easier to compare and the results were easier to interpret.

The mean forecast error* was obtained for the four different ZTH thresholds (25, 30, 35, and 40 dbZ) and 11 different correlation parameter values (1.0 to 3.0 km min^{-1} in steps of 0.2 km min^{-1}) to determine the best value for use in the echo-centroid forecasting program.

---

*Forecast error refers to forecast position error.

5.   RESULTS AND DISCUSSION

a.   Real-Time Analysis

The echo-centroid forecasting program operated satisfactory for 25 storm days in support of JDOP for a total of approximately 170 hours of operation. One of the most impressive performances of the echo-centroid forecasting routine was on 5 April 1978 (Case 1) during real-time operation in support of JDOP (Figs. 14, 15, 16, 17, and 18). All storms had been moving to the northeast, when the echo-centroid forecasting program started to forecast movement of a storm to the east near Lawton, Oklahoma. This information was passed to the NWS, who in turn updated their warning to the public to include those counties to the east of Lawton. A family near Marlow, Oklahoma took shelter based on this warning and later a tornado destroyed their home. Without the use of the real-time echo-centroid forecasting program, this storm movement may have been determined too late.

Operational forecasters during JDOP used the program output to improve their warnings. Ralph Donaldson and Don Burgess, forecasters during JDOP, commended the program on its capability to obtain accurate storm motion and speed information.

The program also showed its capability for identifying

slow moving storms, such as the one on 9 April 1978 (Case 2).
This slow movement, combined with the knowledge of large Z-
weighted areas, indicated the possibility of flash flooding.
On 9 April 1978, the northern most storms had echo-centroid
movements of approximately 1 to 3 m sec^{-1}. This information
enabled the forecasters to advise NWS of the possibility of
flash flooding in this area.

This system should improve the forecaster's ability to
project storm movements and thus reduce the warning area for
severe storms. New public confidence in the warning system
might be achieved and thus eliminate the complacency that
develops from crying "wolf" too often.

b.   Post Analysis

Post analysis was accomplished in order to test the pro-
gram sensitivity to the ZTH threshold and correlation para-
meter. Also, the usefulness of the echo-centroid forecasting
system needed to be stated in quantitative terms.

1) Sensitivity Tests

Different ZTH thresholds were compared to determine the
best value for storm-centroid tracking. The correlation para-
meter was held constant at 2.0 km min^{-1}. The mean forecast
errors (Table 7) for each case were computed from the 12- and
24-min forecast errors for all forecasts made during the col-
lection period. A comparison of the means gave no conclusive
results. The threshold appears to be dependent on the indi-
vidual storm day. For example, 25 dbZ was the best for Case 3,

35 dbZ for Case 2, and 35 dbZ for Case 1. The 40 dbZ threshold was not considered useful for most cases due to the small number of correlations that could be obtained. Thus, only one threshold value, 40 dbZ, was eliminated based on these results.

In order to reach a more conclusive result, the mean forecast errors were computed using the larger Z-weighted areas; only storms with Z-weighted areas of 4000 km^2 or greater were used for this comparison (Table 8). Based on these data, the 30 dbZ threshold was determined to be the best value for Cases 1 and 2, but 25 dbZ remained the best for Case 3. The results for Case 3 were probably due to less shift in the 25 dbZ centroid early in the storm's life. Even though 25 dbZ was the best for Case 3, for general overall operation 30 dbZ should be used. By using 30 dbZ instead of 25 dbZ the more important portions of the storm will be tracked and forecasted.

The sensitivity of the algorithm to the correlation parameter was tested next. The correlation parameter was varied from 1.0 km min^{-1} to 3.0 km min^{-1} in steps of 0.2 km min^{-1}. The mean forecast errors are given in Table 7. All values were compared to the real-time operation value of 2.0 km min^{-1}. The results showed that for values greater than 2.0 km min^{-1}, the forecasts were generally poorer. When values of 2.8 km min^{-1} or greater were used, the forecasts were considerably degraded. For values less than 2.0 km min^{-1}, the forecasts were generally better, but fewer in number. Thus, the storm-centroid track is discontinuous resulting in a loss of

information concerning the centroid movement. Therefore, utilization of 2.0 km min^{-1} for the correlation parameter is justified by the sensitivity tests.

2) Quantitive Analysis

Forecast accuracy was also a part of the post analysis. The overall accuracy for each day was computed as well as the accuracy for several selected storms on each individual day. The overall mean forecast position error for Cases 1, 2, and 3 was 9.96 km, 11.64 km, and 12.59 km, respectively. These values are for the 12- and 24-min forecasts combined. The individual 12- and 24-min mean forecast errors are shown in Table 9. As expected, the 12-min forecast is much better than the 24-min forecast for each case. The tracks for Cases 1, 2, and 3 are shown in Figs. 19a, 19b, 20a, 20b, 21a, and 21b.

The individual errors varied from slightly better to slightly poorer than the overall error. For Case 1, the Marlow, Oklahoma tornado storm centroid showed a 12- and 24-min mean forecast error of 4.39 km and 6.42 km, respectively. The combined mean forecast error was 5.43 km (Table 10). The time series plot of the forecast errors are shown in Fig. 22. The peak at 2156 CST appears to be caused by a change in the centroid motion from a easterly movement to slightly northeasterly.

A storm located approximately 230 km to the south of Norman was also examined for Case 1. The large forecast errors (Fig. 23) between 2107 and 2144 CST were a result of the centroid calculations made as the storm was moving within

the maximum radar range of 230 km. The actual centroid was not obtained until the complete echo moved within the radar's range. Thus, a pseudo centroid position lead to the large forecast errors. Once the actual storm centroid was within range, it was then tracked with improved forecast accuracy.

For Case 2, two separate storms were also investigated. One storm produced heavy rain, while the other produced a mesocyclone. The 12- and 24-min mean forecast errors for the heavy rain storm were 11.38 km and 12.60 km, respectively (Table 10). The time series plot in Fig. 24 suggests that when centroids are slow moving and shifting around, forecast positions are not very accurate. Although these positions were not as accurate as those for Case 1, the speed information was very useful. The slow speed alerted the forecaster to the possibility of heavy rains and flash flooding.

For the mesocyclone storm in Case 2, the 12- and 24-min forecast errors were 10.46 km and 13.37 km, respectively (Table 10). From the time series plot in Fig. 25, the larger errors around 1830 CST were due to very large centroid shifts on the order of 20 km. These shifts may be due to certain dynamics within the storm (e.g., development of initial storm rotation) (Donaldson, 1979).

The last storm (known as the Piedmont storm) examined produced the tornado that hit northwest Oklahoma City (Case 3). The mean forecast errors were 7.73 km and 17.66 km for the 12- and 24-min forecasts, respectively (Table 10). The time series

plot of this storm is presented in Fig. 26. The large error at 1739 CST was due to a forecast based on only 2 observations. The centroid shift was again about 20 km. This apparent storm movement led to several bad forecasts until there were enough observations to overcome the initial error. The storm centroid moved very little for about the first 40 minutes. The storm then moved toward the northeast. The slow movement, along with the initial large centroid shift, resulted in large forecast errors. Thus, the 12-min forecast was much better than the 24-min forecast. Once the storm started moving (after 1818 CST) the mean forecast error for the 12-min forecast was 5.59 km.

Finally, the comparison was made between the number of observations used to obtain the forecast and the forecast error. This information is plotted in Fig. 27 using Table 11. It is apparent that after five observations are obtained, the forecast error drops considerably. The normal lifetime of an echo (25 to 30 min) is reflected by the maximum in the sample size at 4 observations. Only the larger, more consistent storms have more than an hour's worth of observations to forecast its centroid movement. Thus, the program shows increased forecast accuracy when used to track the larger, more intense storms.

6.   CONCLUSIONS AND FURTHER STUDIES

a.   Conclusions

The echo-centroid forecasting program has proven to be
a valuable analysis and forecast tool. Its capability to fore-
cast centroid movements was proven by its real-time applica-
tion during JDOP 1978. Post analysis, accomplished for three
storm days, revealed an overall mean forecast error of approx-
imately 10 km. This error was only 5 km for two individual
severe storms. Thus, this system could be used to improve
the quality of severe storm warnings by accurately forecast-
ing the severe storm-centroid positions.

The optimum ZTH threshold for storm-centroid forecasting
is approximately 30 dbZ with a correlation parameter of 2.0 km
min^{-1}. The 40 dbZ threshold is not recommended for use at the
lowest elevation angle. Correlation parameter values of 2.8
and 3.0 km min^{-1} are too large for program use.

The time series plots clearly point to the need for some
subjectivity in the determination of those forecasts that are
obviously "in error" due to severe centroid shifts. These
shifts might be a clue to certain dynamical changes occurring
within the storm.

In conclusion, the usefulness of a real-time echo-
centroid forecasting program has been proven. The forecaster

has been supplied with a new dimension to real-time severe storm analysis and forecasting.

b.   Suggestions for Further Study

Program sensitivity to the elevation angle used for gathering the data should be investigated. This would optimize this portion of the program. An effort is already under way at AFGL to expand this method to one using a three-dimensional centroid. Operational testing will be conducted during AFGL's 1979 spring program at Norman, Oklahoma. These results should be compared to the two-dimensional case to determine the effect of the extra dimension on the forecast accuracy.

Program sensitivity to the weighting of observations used to make a forecast should also be explored. Several different schemes could be used including the one employed by Zittel. One scheme might involve leaving the weighting factor at one, but using only the last 4, 5, or 6, etc. observations.

The problems that result when a storm enters or leaves the maximum radar range should be studied. Methods for correcting these and other obvious forecast errors should be explored. An automated method might be used, but at the very least, an interactive method should be employed.

How the storm dynamics are related to storm-centroid shifts and to slow movement should also be addressed. Subjectively, these movements appear to be indicators of developing mesocyclones and storm intensification.

The final area of further study should be software optimization. This optimization would allow for further improvements such as mesocyclone identification and tracking to be implemented using existing hardware.

BIBLIOGRAPHY

Austin, G. L. and A. Bellon, 1974: The use of digital radar records for short term precipitation forecasting. Quart. J. R. Met. Soc., 100, 33-39.

Barclay, P. A. and K. E. Wilk, 1970: Severe thunderstorm radar echo motion and related weather events hazardous to aviation operations. ESSA Tech Memo., ERL-NSSL 46, 63 pp.

Bjerkaas, C. L., 1977: Mesoscale characteristics of precipitation in a disturbance over the tropical Eastern Atlantic. S. M. Thesis, Dept. of Meteor., MIT, 105 pp.

Blackmer, R. H., Jr. and R. O. Duda, 1972: Application of pattern recognition techniques to radar data. Preprints 15th Radar Meteor. Conf., AMS, Boston, Mass., 138-143.

_____, R. O. Duda, and R. Reboh, 1973: Application of pattern recognition techniques to digitized weather radar data. Final Report Contract 1-36072, SRI Project 1287, Stanford Research Institute, Menlo Park, Cal., 89 pp.

Boak, T. I. S., III, A. J. Jagodnik, Jr., R. B. Marshall, D. Riceman, and M. J. Young, 1977: Tracking and significance estimator. R & D Equipment Information Report, Contract AFGL-TR-77-0259, Raytheon Company, Wayland, Mass., 118 pp.

Donaldson, R. J., 1979: Private communication.

Elvander, R. C., 1976: An evaluation of the relative performances of three weather radar echo forecasting techniques. Preprints 17th Radar Meteor. Conf., AMS, Boston, Mass., 526-532.

Hilst, G. R. and J. A. Russo, Jr., 1960: An objective extrapolation technique for semi-conservative fields with an application to radar patterns. Tech. Memo. No. 3, Contract AF30-631014459, The Travelers Weather Research Center, Inc., Hartford, Conn., 34 pp.

Newton, C. W. and J. C. Fankhauser, 1964: On the movements of convective storms, with emphasis on size discrimination in relation to water-budget requirements. *J. Appl. Meteor.*, *3*, 651-668.

Staff of National Severe Storms Lab, Environmental Research Lab-Weather Radar Branch, Air Force Geophysics Lab-Equipment Development Lab, National Weather Service, Air Weather Service, and United States Air Force, 1979: Unpublished Final Report on the Joint Doppler Operational Project (JDOP), 1976-78.

Wilk, K. E. and K. C. Gray, 1970: Processing and analysis techniques used with the NSSL weather radar system. Preprints 14th Radar Meteor. Conf., AMS, Boston, Mass., 369-374.

Wilson, J. W., 1966: Movement and predictability of radar echoes. ESSA Tech Memo., ERLTM-NSSL 28, 30 pp.

Zittel, W. D., 1976: Evaluation of a remote weather radar display, Vol II-Computer applications for storm tracking and warning. Final Report Contract DOT:FA74WAI-440, Report No. FAA-RD-76-60, II, NSSL, Norman, OK, 114 pp.
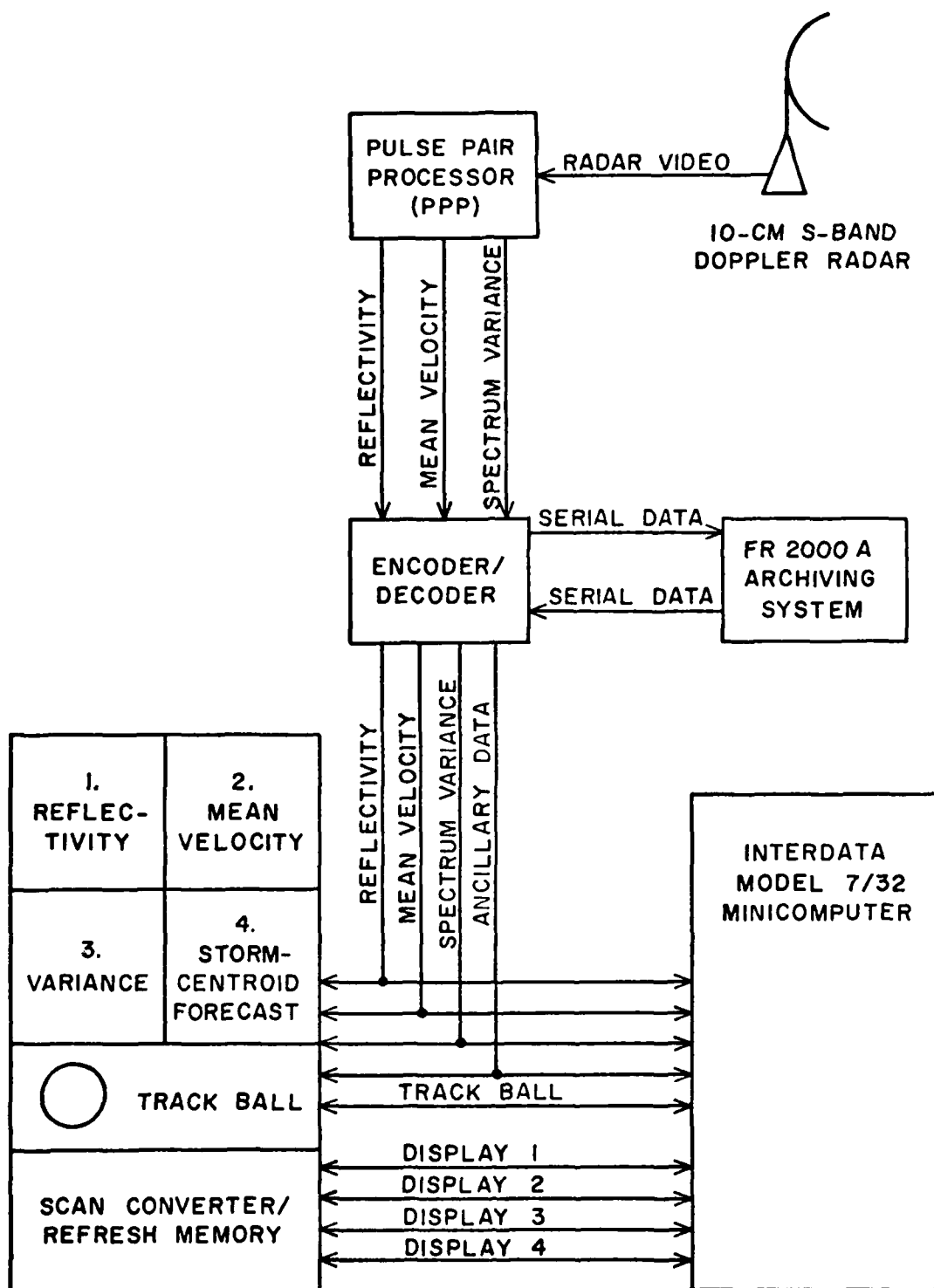
Fig. 1. System block diagram.
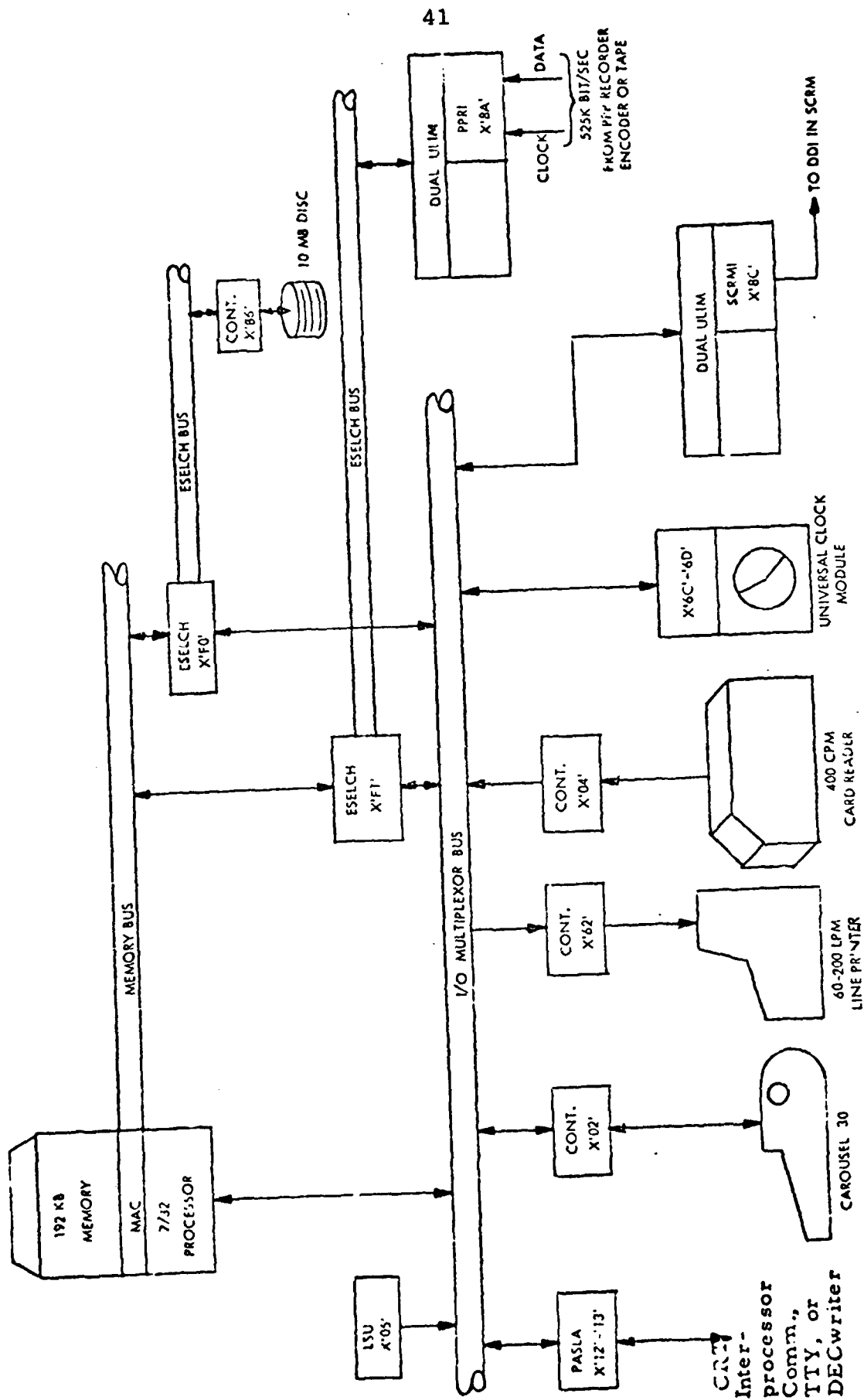
Fig. 2.   Computer Block Diagram (Bork, et al., 1977).
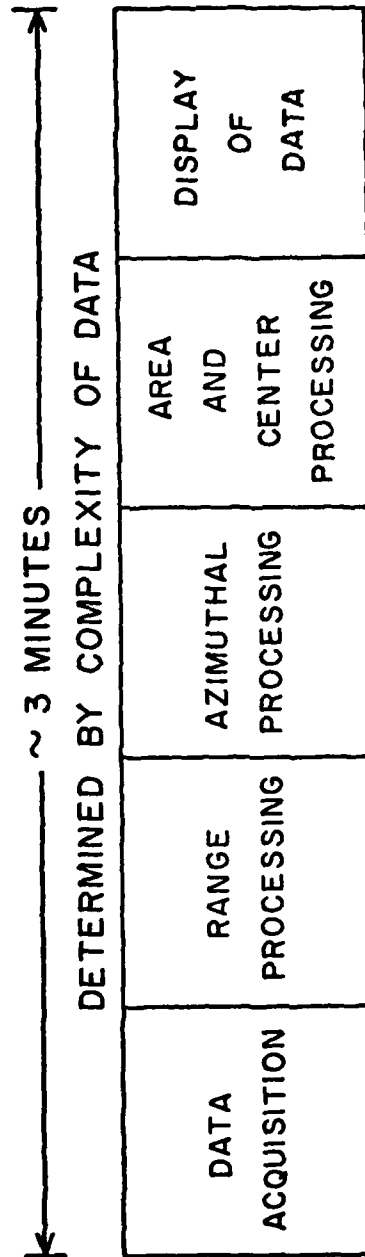
Fig. 3. Software timing diagram. Blocks are not proportional to processing time (Boak, et al., 1977).

REFLECTIVITY ABOVE ZTH
OVLP = 2

AZIMUTHS

AZIMUTHS

Example I.
Considered part of same
storm segment

Example 2.
Considered two separate
storm segments
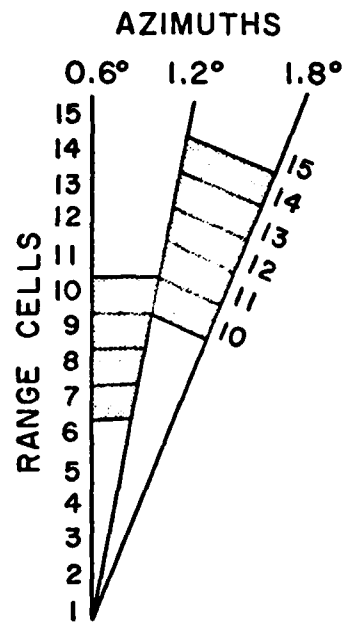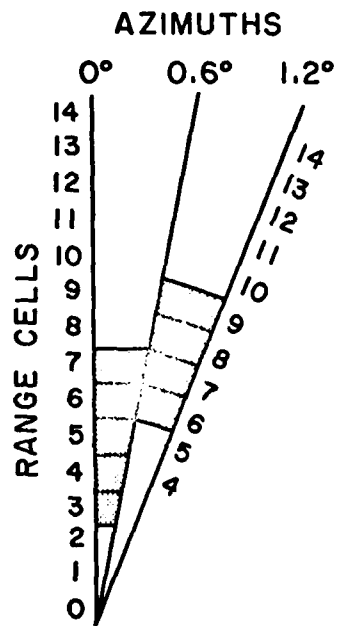
Fig. 4. Overlap criterion for determination of
storm segments. Range threshold (RHO) is 3 range
cells and OVLP is 2 range cells.
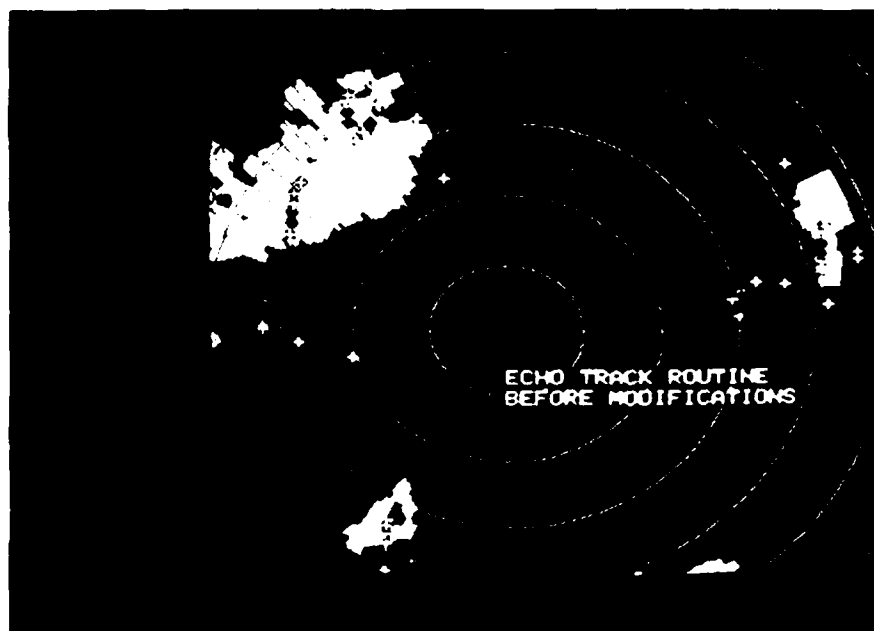
Fig. 5. Raytheon data presentation before modifications. The "+" locates the various centroid locations (past and present) and its color corresponds to the various acquisition times. The solid area is the current echo outline above the reflectivity threshold (ZTH).

Y

Old Time 1200 CST
New Time 1206 CST
2.0 km min⁻¹ Correlation Parameter

25 km

Old
Centroid
Position
20 km   X A₁
Uncorre-
lated

15 km   New
                                   Centroid
                                   O   B₂
                                   Position

10 km

                        Old
                      Centroid
                      Position
 5 km   X B₁
                      Correlated

0,0   5 km   10 km   15 km   20 km   25 km   30 km
                                                      X
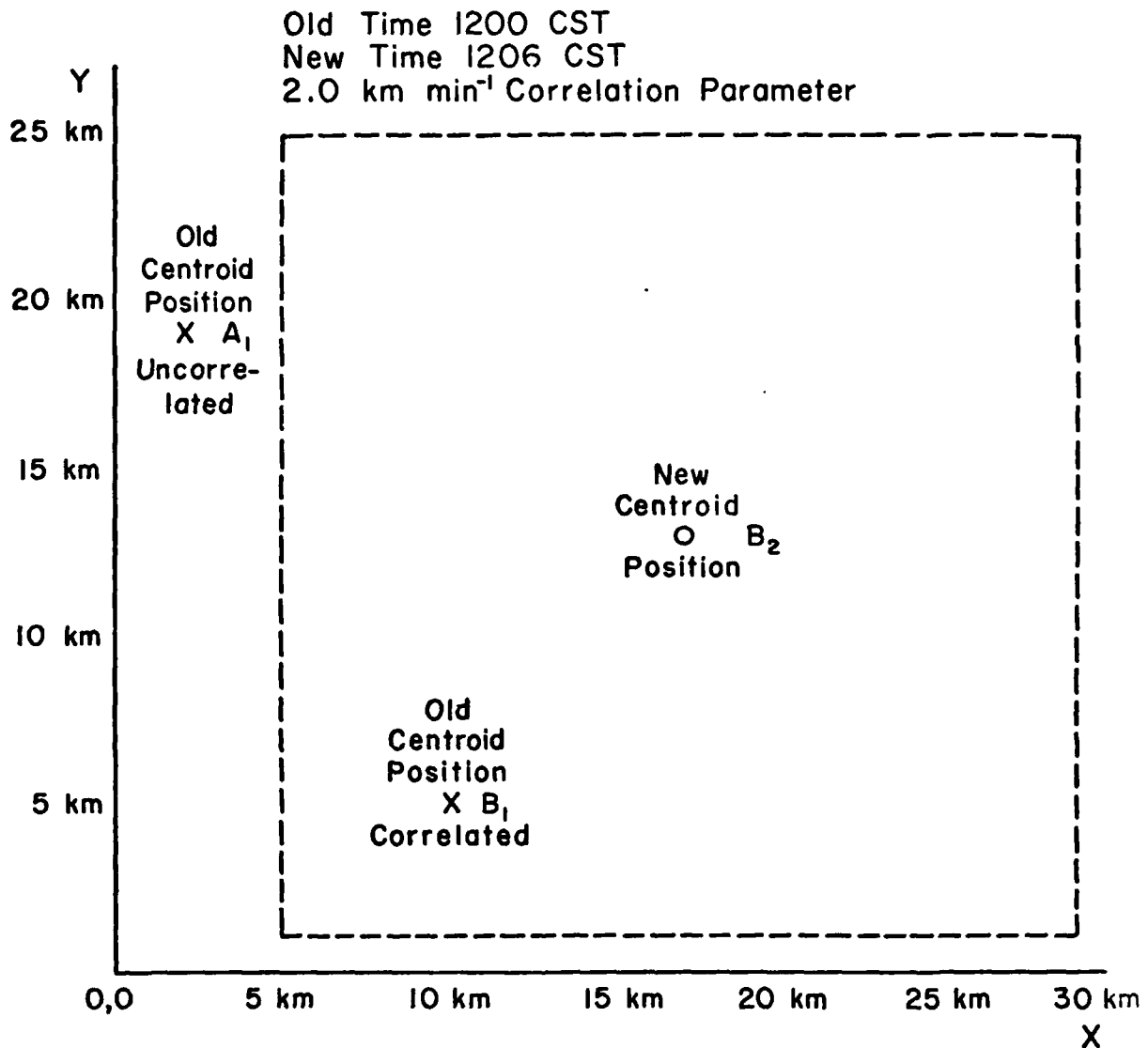
⌐---⌐
| | — Any Centroid inside this box will
L---J   correlate with New Centroid Position

        For this case it is a box 24 km
        square centered on the New Centroid
        Position

Fig. 6. Illustration of Correlation Algorithm. A_1 and B_1
correspond to storms at 1200 CST, while B_2 is storm at
1206 CST. Radar origin is at $X = 0$, $Y = 0$. Correlation
parameter (DCOR) is 2.0 km min⁻¹.

A - 12-minute forecast based on previous
    Centroid Position

B - Actual Centroid Position after 13
    minutes

C - 13-minute forecast based on previous
    Centroid Position

O - Previous Centroid Position
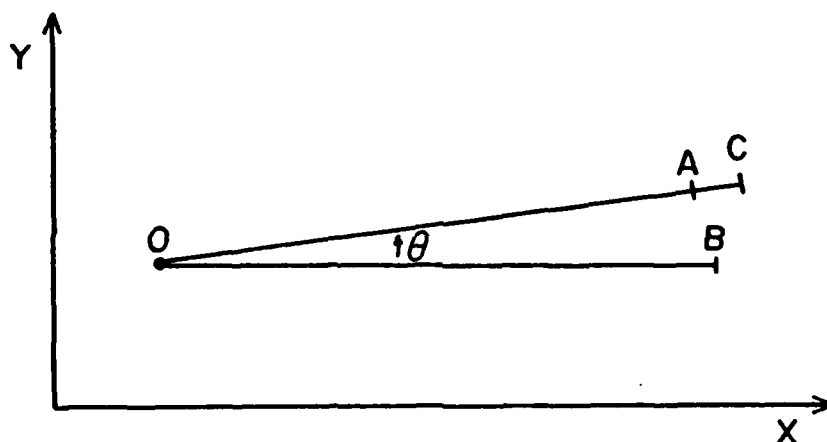
$$\text{Speed Error} = \frac{BO - CO}{13} \ \text{km/min}$$

$$\text{Direction Error} = \frac{\theta}{13} \ \frac{\text{degrees}}{\text{min}}$$

Fig. 7. Illustration of speed and direction
error. The storm centroid has moved from
point O to point B in last 13 minutes. Point
A is 12-min forecast position obtained when
centroid was at point O. Point C is 13-min
forecast position from original point O.
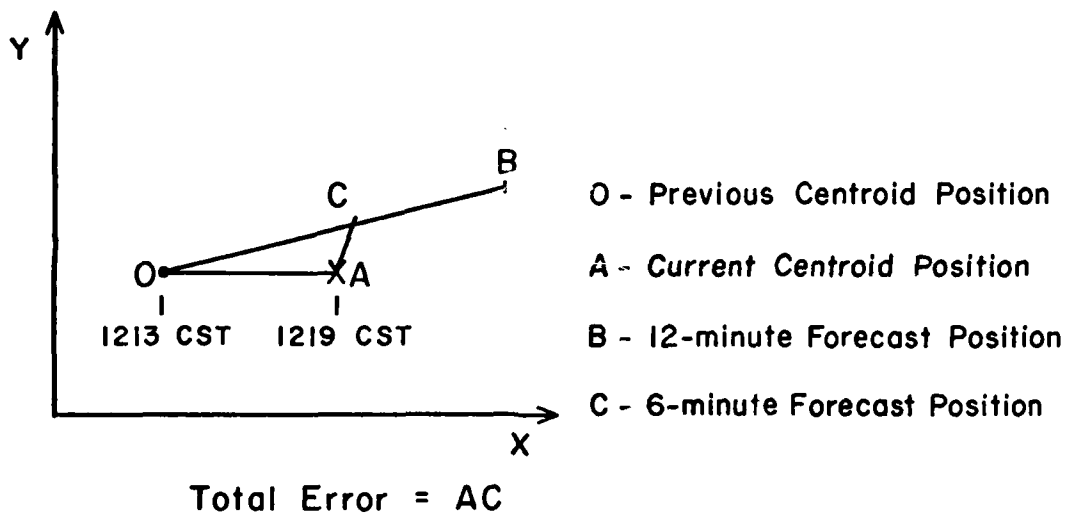
Total Error = AC

Fig. 8. Illustration of total error used for real-time
operations. The storm centroid has moved from point O
to Point A. Its 6-min forecast position is point C.
Total error equals distance AC.
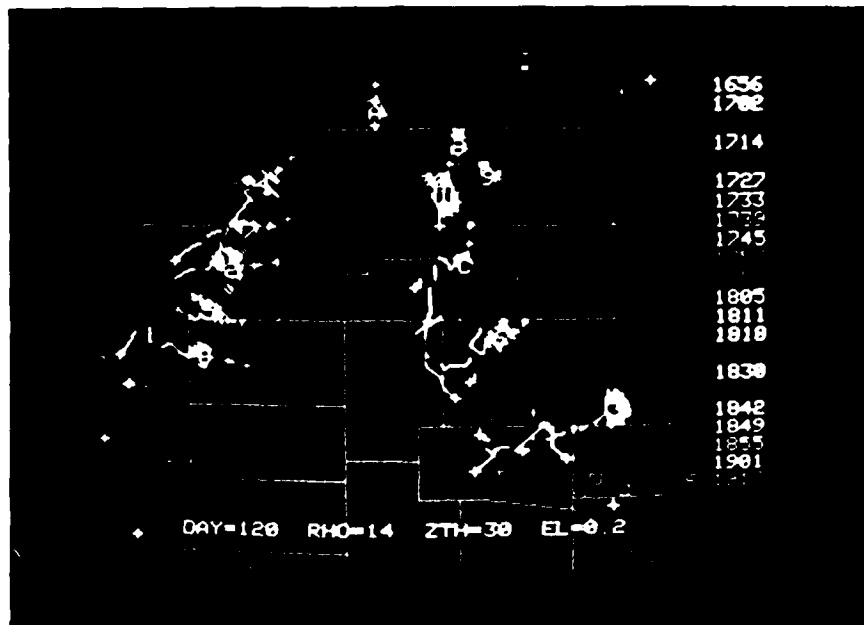
Fig. 9.   Data presentation after modifications.
The "+" locates the initial centroid position and
the forecast positions. The "+'s" and lines are
color coded according to their acquisition times
located in the legend. F's on the legend repre-
sent valid times of the forecasts. Hexadecimal
numbers correspond to rank of Z-weighted area
(1 being the largest). Overlay is of north cen-
tral Oklahoma. Time of observation is 1901 CST
on 30 April 1978. Elevation angle of 0.2 degrees.

```
NO. RANGE CELLS:  14  GRND:  53  OVERLAP:  5  IPRFM: 1
PRF CODE:1    DB:65.28    BITVEL:34.24    BITSTD:15.41

DATE:120 TIME:1836 ELEVATION: 0.4 COLOR: E ZTHRES: 30
```

AREA	1	2	3	4	5	6	7	8	9	A	B	C
RANGE (KM)	150	218	104	212	214	54	220	216	222	128	210	116
AZIMUTH (DEG)	331	313	330	302	296	348	10	307	351	327	1	332
AREA (KM**2)	340	232	160	164	156	148	100	92	56	36	28	24
MAX REFLCT (DBZ)	52	48	53	45	44	49	40	42	47	40	40	53
MAX VEL (M/S)	24	13	17	17	12	26	18	14	16	10	14	9
MAX VEL SD (M/S)	14	11	8	9	8	12	10	10	10	9	8	7
MASS (DBZ KM**2/10)	1424	944	664	632	620	608	416	356	252	148	120	112
SPEED (M/S)	16	16	8	999	10	2	999	20	999	10	999	999
DIRECTION (DEG)	174	234	235	999	245	257	999	236	999	225	999	999

```
....................................FORECAST 1....................................
```

AREA	1	2	3	4	5	6	7	8
RANGE (KM)	161.90	216.38	105.55	0.00	209.21	54.59	0.00	212.81
AZIMUTH (DEG)	332.80	315.37	332.95	0.00	297.30	351.57	0.00	310.43
DIR ERR (DEG/MIN)	29.22	0.00	-0.64	0.00	0.00	-0.48	0.00	0.00
SPEED ERR (KM/MIN)	0.20	0.00	0.10	0.00	0.00	-0.57	0.00	0.00
TSD (KM)	0.83	2.19	7.42	0.00	12.95	2.09	0.00	4.00

```
...........................FORECAST 2...........................
```

AREA	1	2	3	4	5	6	7	8
RANGE (KM)	173.53	213.93	106.62	0.00	205.91	54.33	0.00	209.32
AZIMUTH (DEG)	334.03	318.41	336.80	0.00	299.05	353.66	0.00	314.23
DIR ERR (DEG/MIN)	13.32	0.00	-0.87	0.00	0.00	-0.87	0.00	0.00
SPEED ERR (KM/MIN)	-0.12	0.00	-0.14	0.00	0.00	-0.51	0.00	0.00

Fig. 10. Storm characteristic list. Area number (1 through C) is the storm number. This hexadecimal number is the same number on the CRT display. This list is for data collected on 30 April 1978 valid at 1836 CST. Number of range cells (RHO) equals 14, ground clutter elimination (GRND) is the first 53 range cells, and overlay criterion (OVLP) is 5 range cells. The maximum range of the radar is 230 km (IPRFM equals 1 for 230 km and 2 for 460 km), and the PRF is 1302 Hz (PRF Code 1). DB, BITVEL and BITSTD are conversion factors for the CRT displays. The elevation angle is 0.4 deg with a reflectivity threshold (ZTH) (denoted by ZTHRES) of 30 dbZ. Color (E - Red-orange) is the color of the numbers on the CRT display for the current acquisition time (1836 CST). Forecasts 1 and 2 are the 12- and 24-min forecasts, respectively. The range and azimuth are the new forecast position, while the error data are for the forecasts valid at 1836 CST.
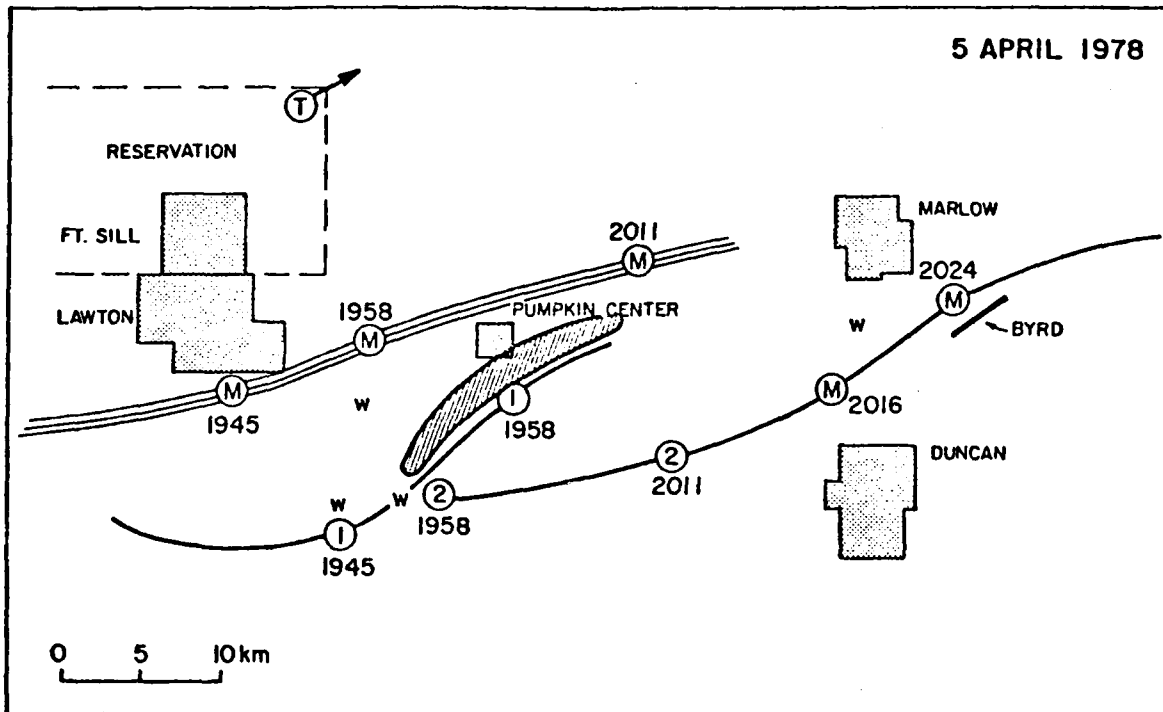
Fig. 11. Track of 5 April 1978 mesocyclone (M) and two TVS's
(1) and (2). Times are CST. Pumpkin Center tornado is hatched
and Marlow tornado is thick line. The circled "T" indicates
tornado position given in NWS warning and W's are straight wind
damage (Staff of NSSL, et al., 1979).
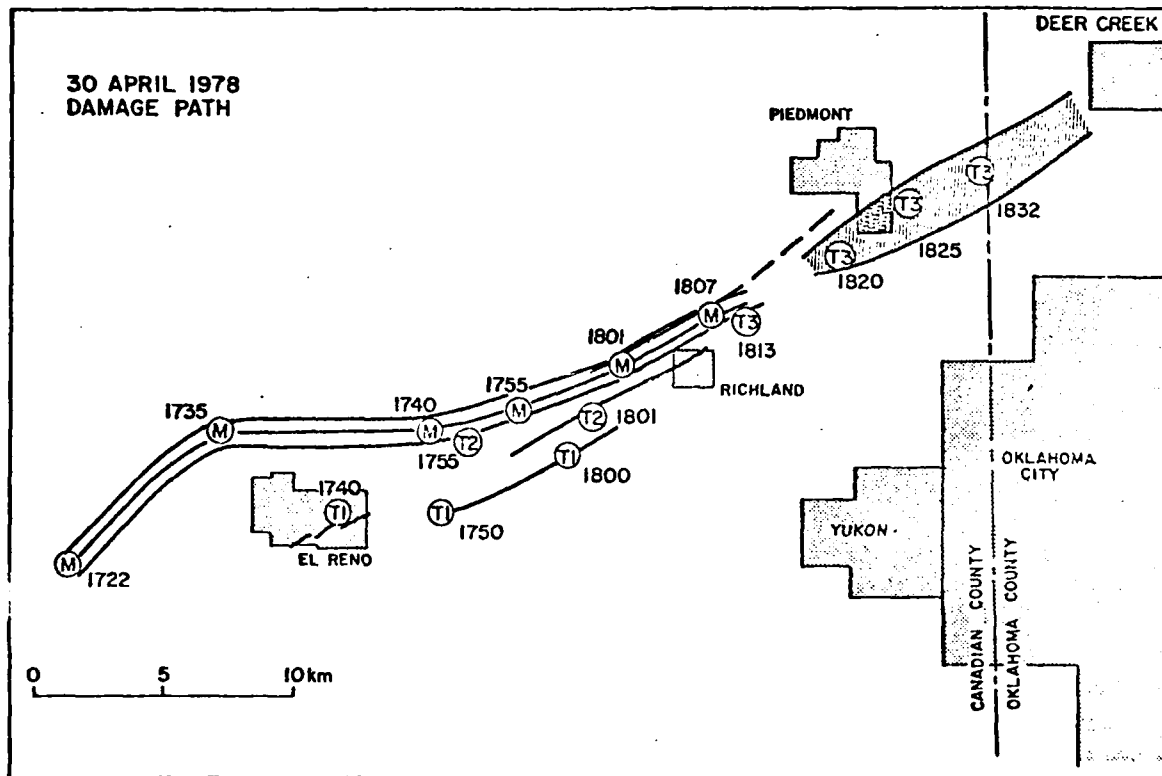
Fig. 12. Damage path of 30 April 1978 Piedmont storm. Thin solid lines indicate small tornadoes on the ground with hatched area marking maxi-tornado swath. Mesocyclone center (M) and TVS' (T1, T2, T3) are located from Doppler data used in real time (Staff of NSSL, et al., 1979).

Y

A C

O

B

1200 CST

1213 CST

X

A - 12-minute forecast
Centroid Position

B - Actual Position at
1213 CST

C - 13-minute forecast
based on coefficients
used to make forecast
at 1200 CST

O - Centroid Position at
1200 CST
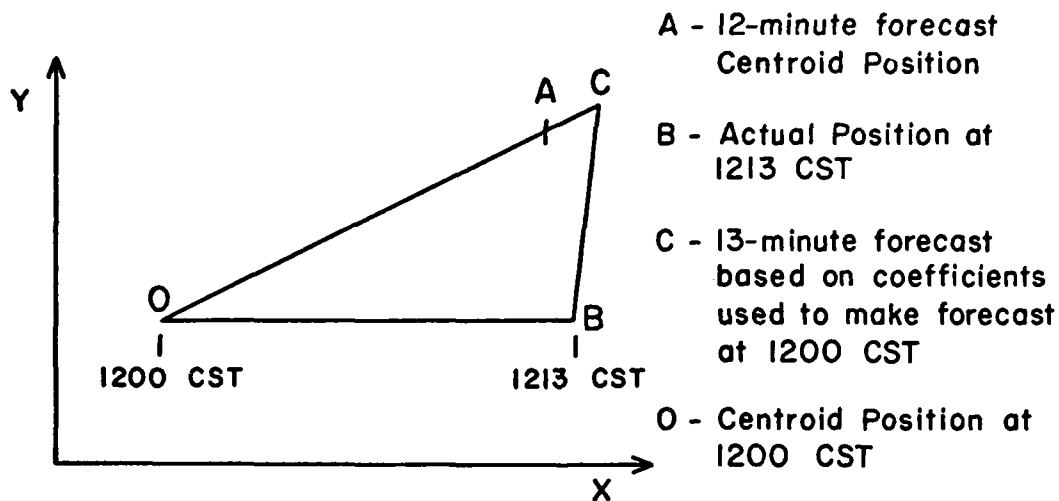
Forecast Error = BC

Fig. 13. Illustration of forecast error used in post
analysis. The storm centroid moved from point O to
point B during last 13 minutes. Point A is the 12-
min forecast position and point C the 13-min forecast
position. The distance BC is the forecast error.

Fig. 14.   Echo track valid at 1913 CST on 5 April
1978.
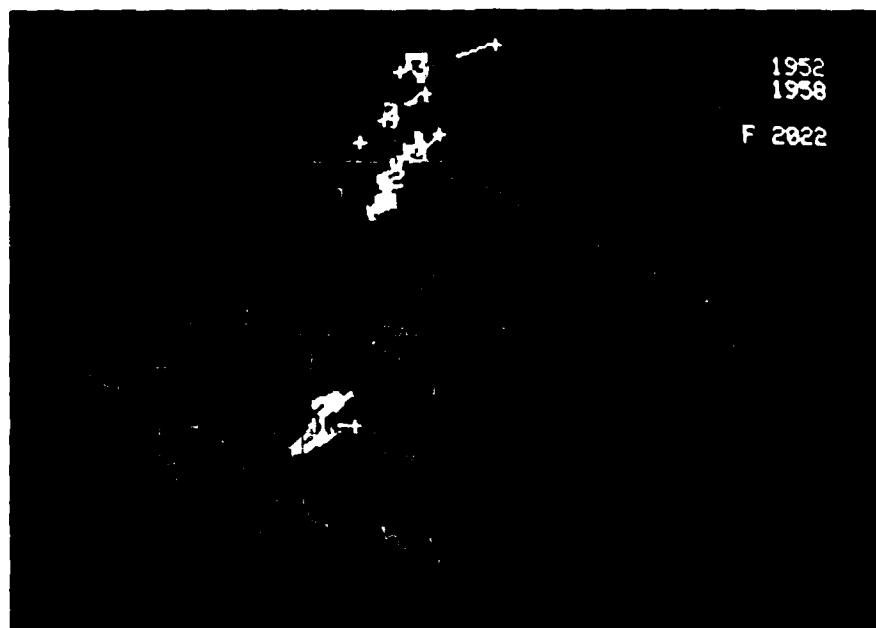
Fig. 15.   Echo track valid at 1958 CST on 5 April
1978.
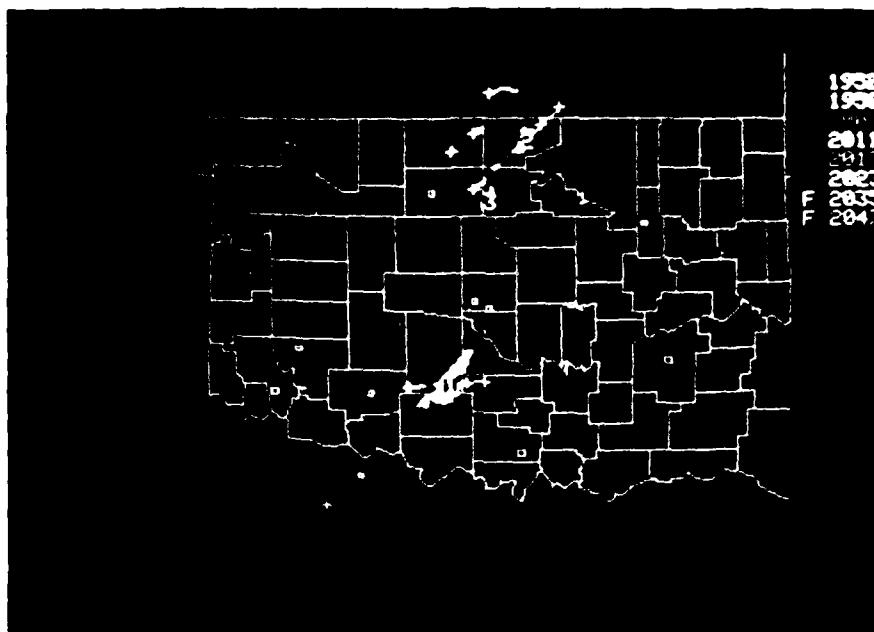
Fig. 16. Echo track valid at 2023 CST on 5 April 1978. Storm 1 produced the Marlow tornado.
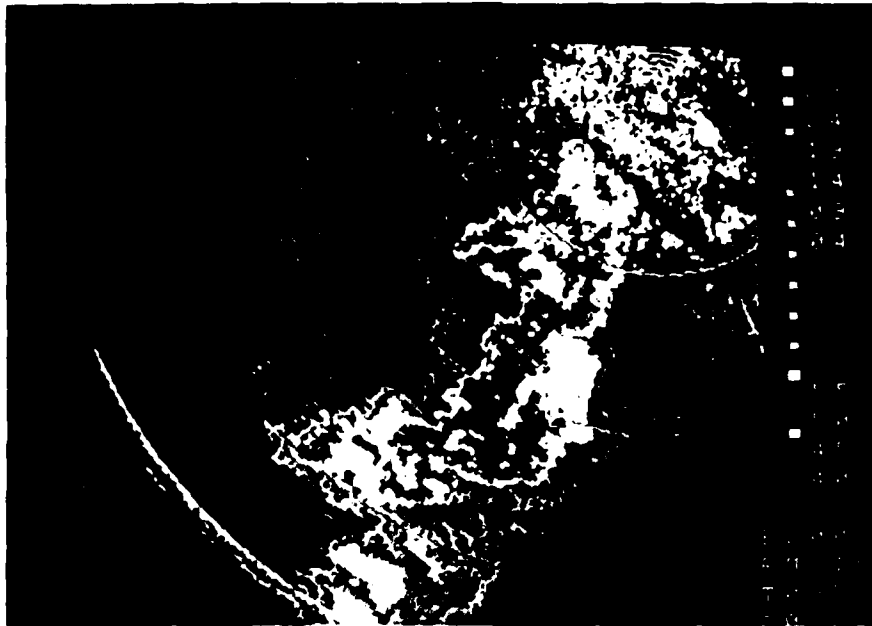
Fig. 17. Reflectivity pattern valid at 2023 CST on 5 April 1978. Classical hook pattern is shown in the approximate location of the Marlow tornado.
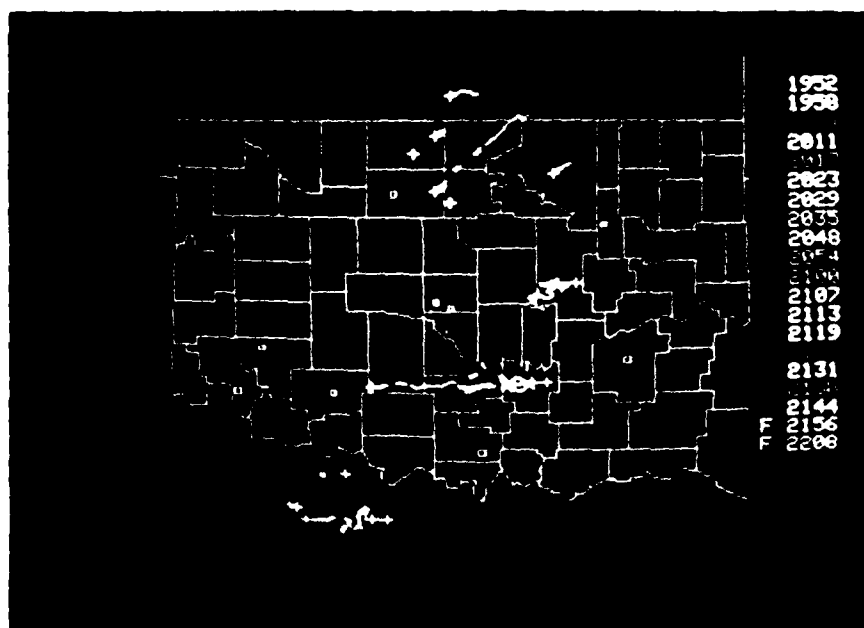
Fig. 18. Echo track valid at 2144 CST on 5 April
1978. Storm 2 is the storm that produced the
Marlow tornado.
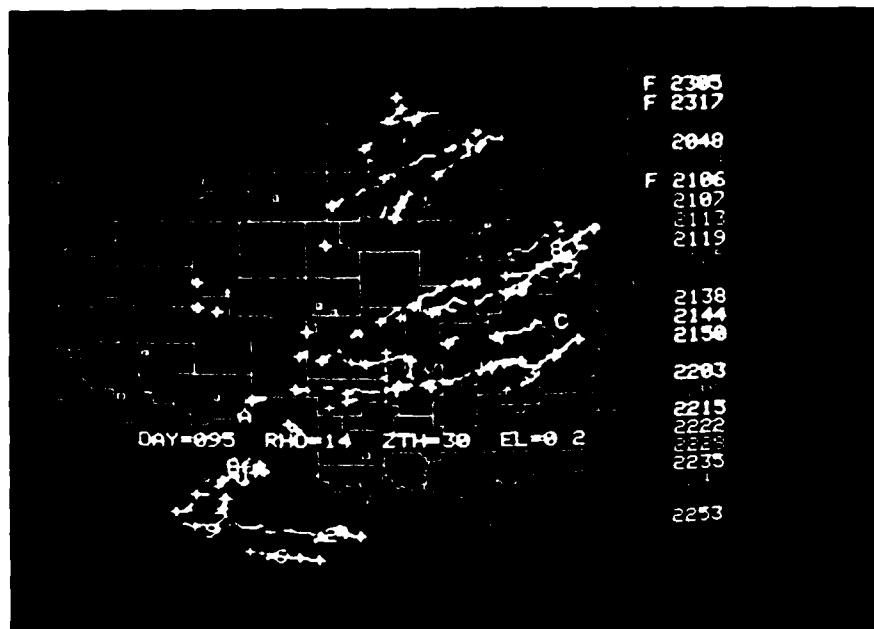
Fig. 19a. Echo track valid at 2253 CST on 5 April 1978. Storm 4 produced the Marlow tornado.
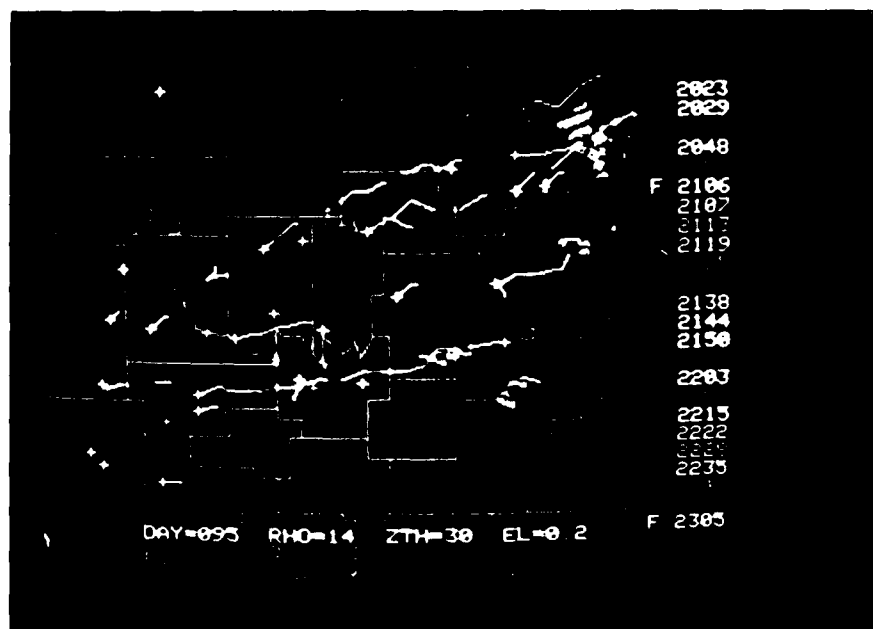
Fig. 19b. Fig. 19a enlarged and valid at 2241 CST. Storm 5 produced the Marlow tornado.
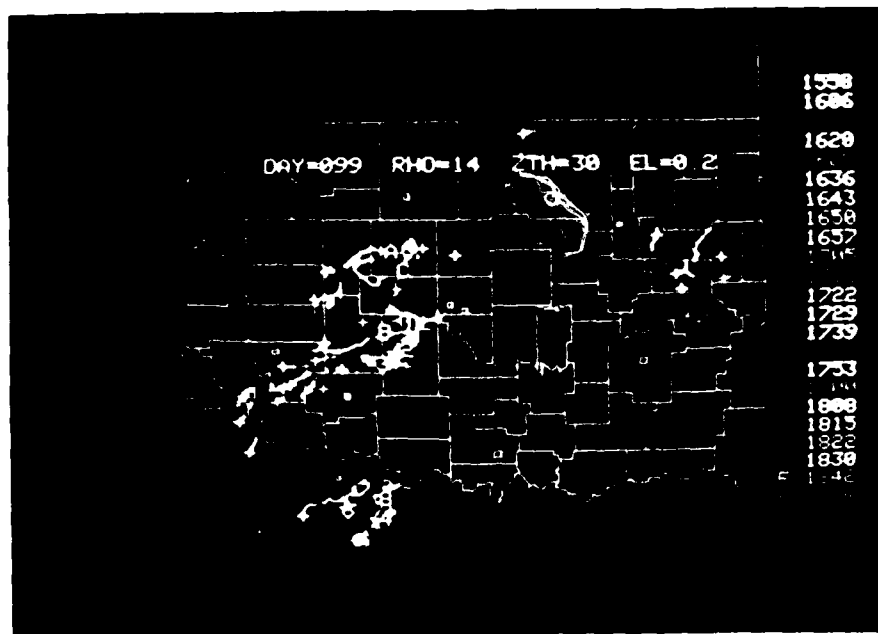
Fig. 20a. Echo track valid at 1830 CST on 9 April
1978 (CASE 2). Storm A produced heavy rain and
Storm 1 produced the mesocyclone.
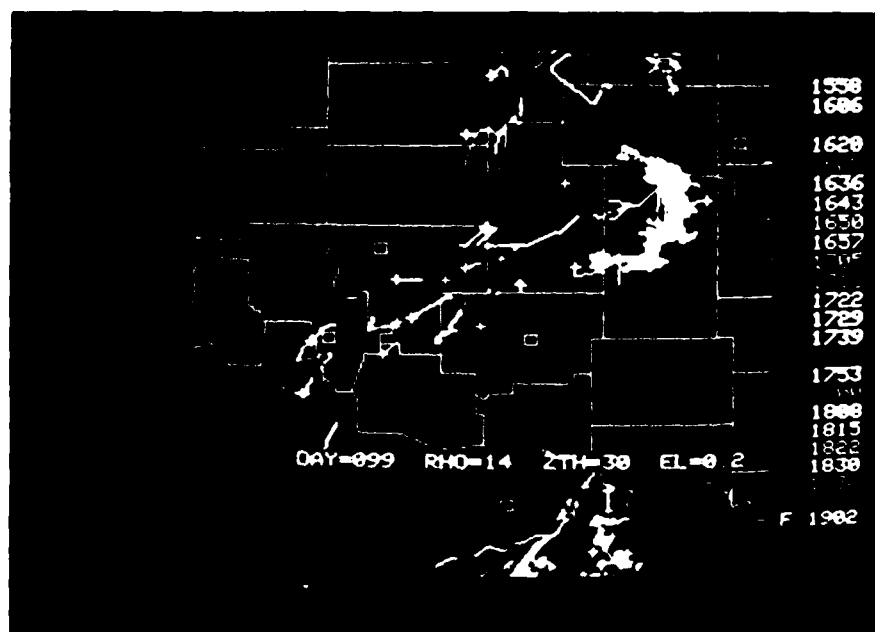
Fig. 20b. Fig. 20a enlarged and valid at 1838 CST.
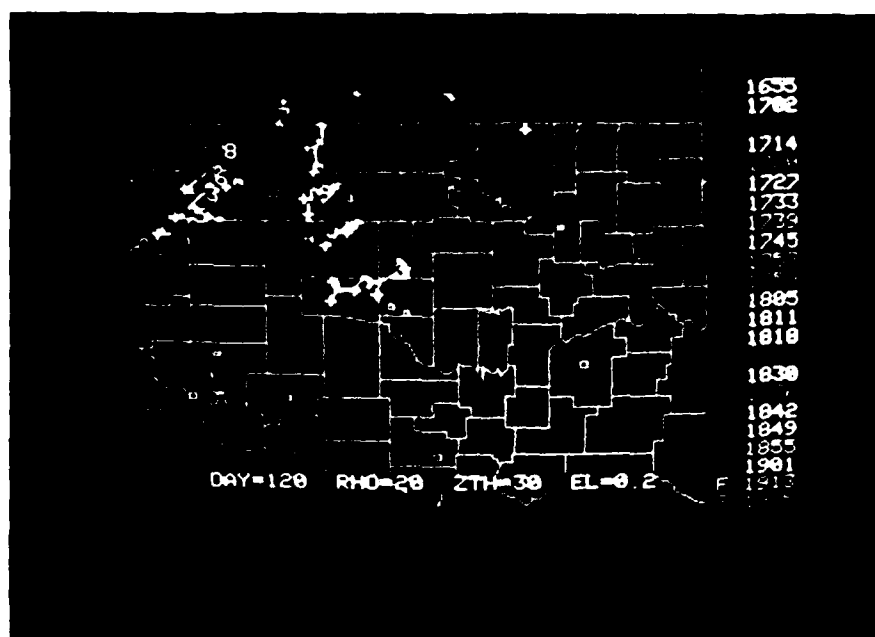
Fig. 21a.   Echo track valid at 1901 CST on 30 April
1978.   Storm 2 produced the Piedmont tornado.
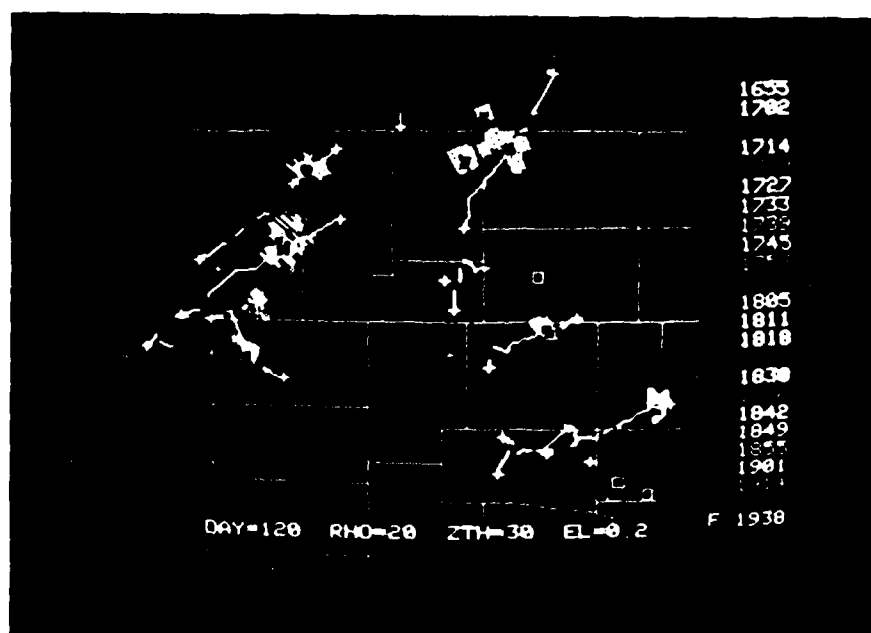
Fig. 21b.   Fig. 21a enlarged.   Valid at 1914 CST.
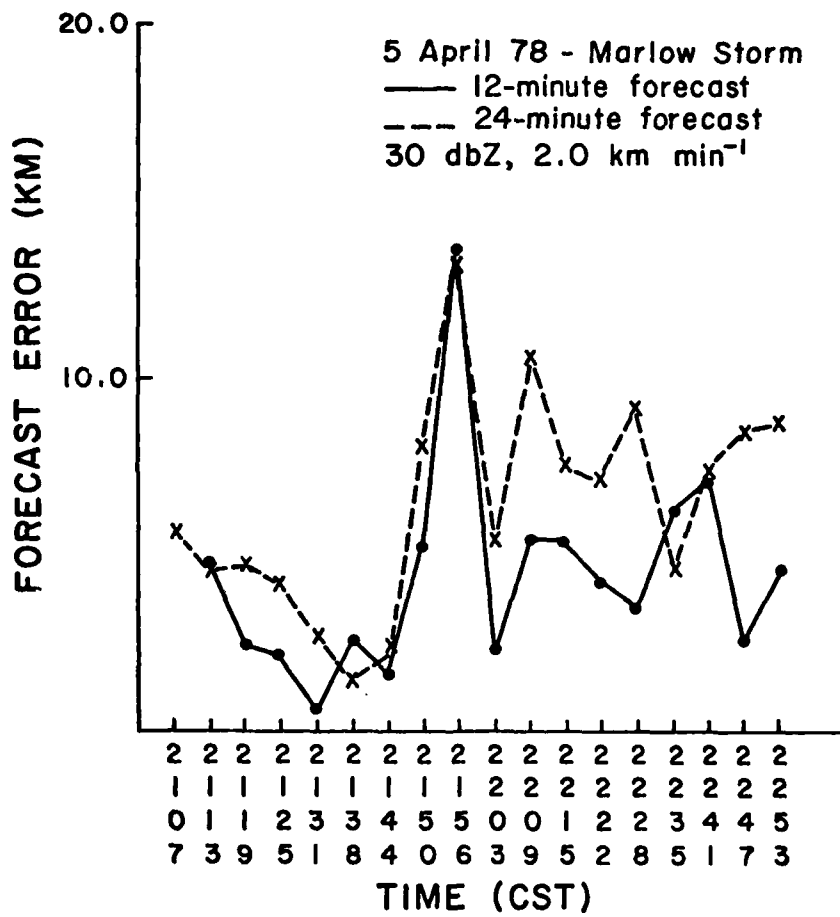
Fig. 22. Forecast errors for the storm producing the Marlow tornado.
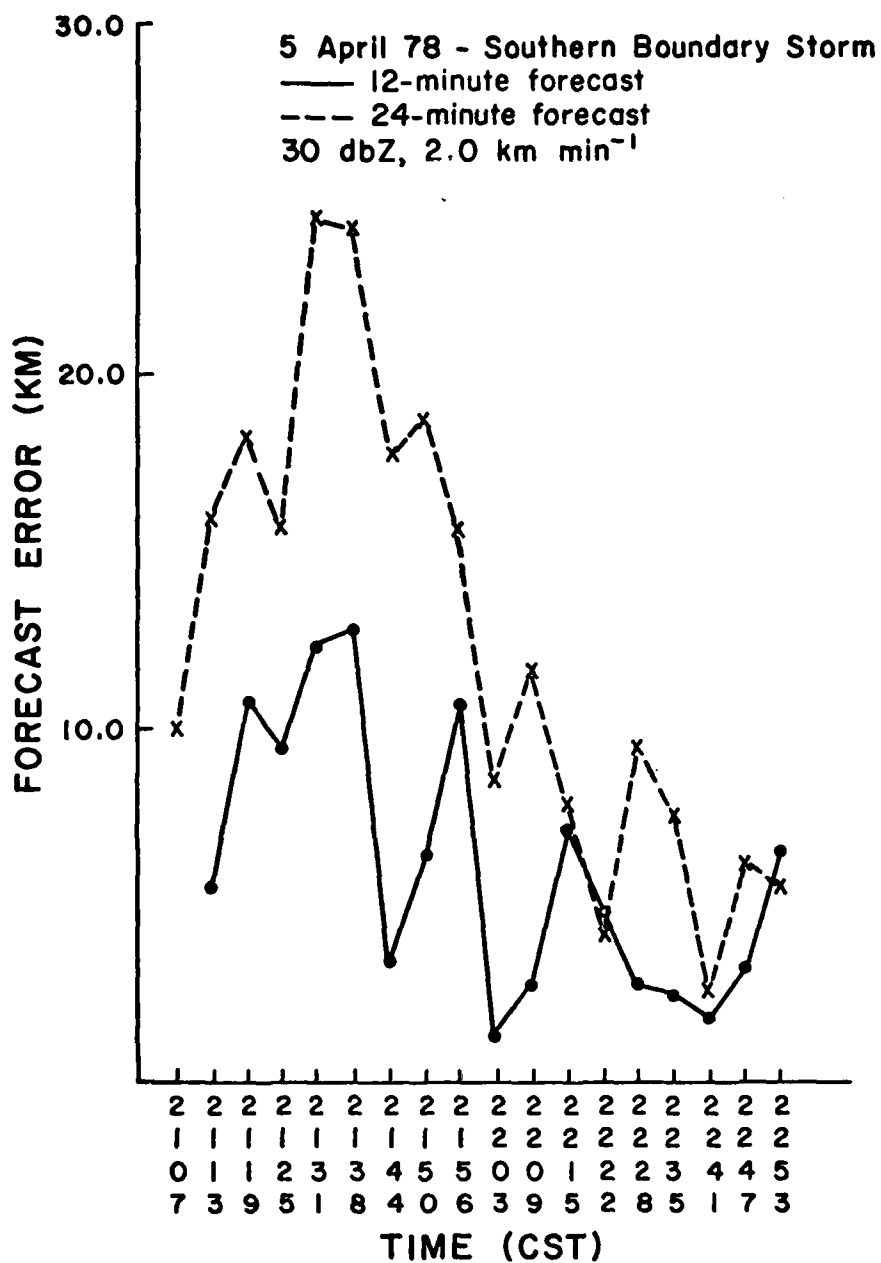
Fig. 23. Forecast errors for the storm on the Southern boundary of the radar's maximum range (230 km).
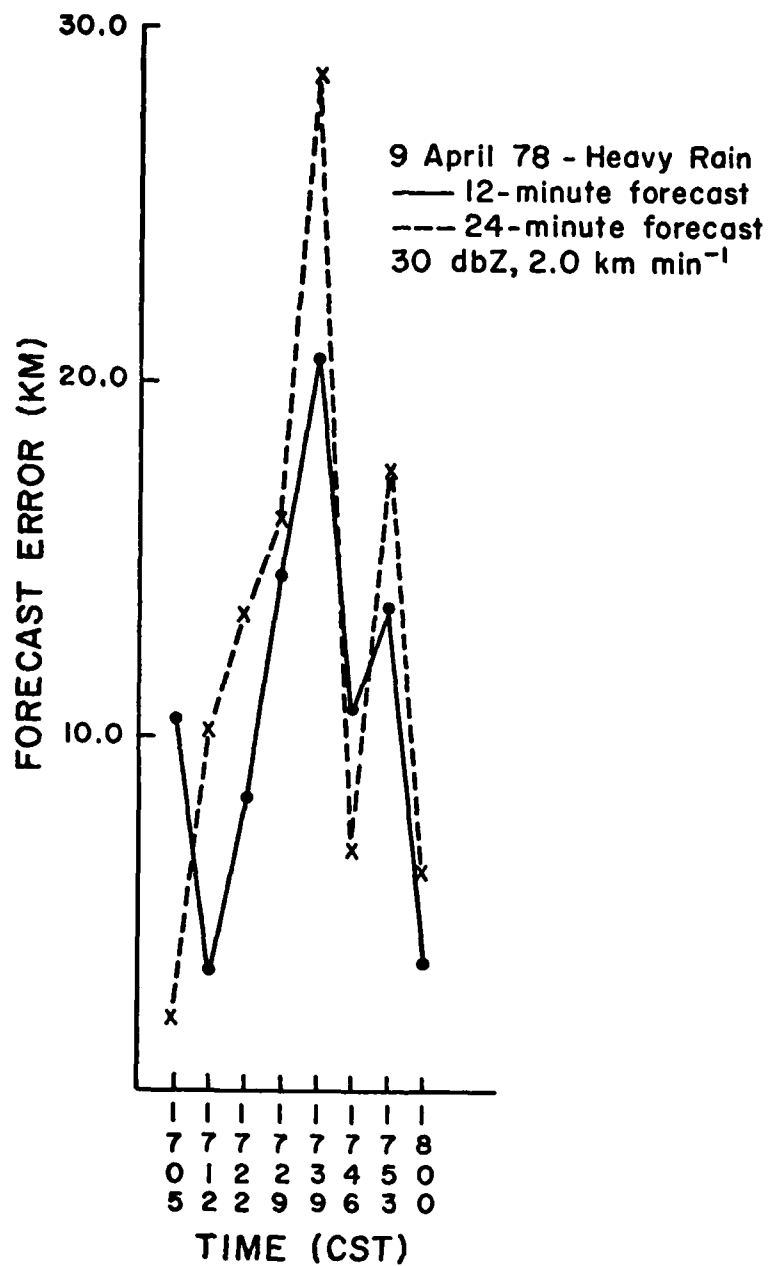
Fig. 24. Forecast errors from the 9 April
1978 storm that produced heavy rain.
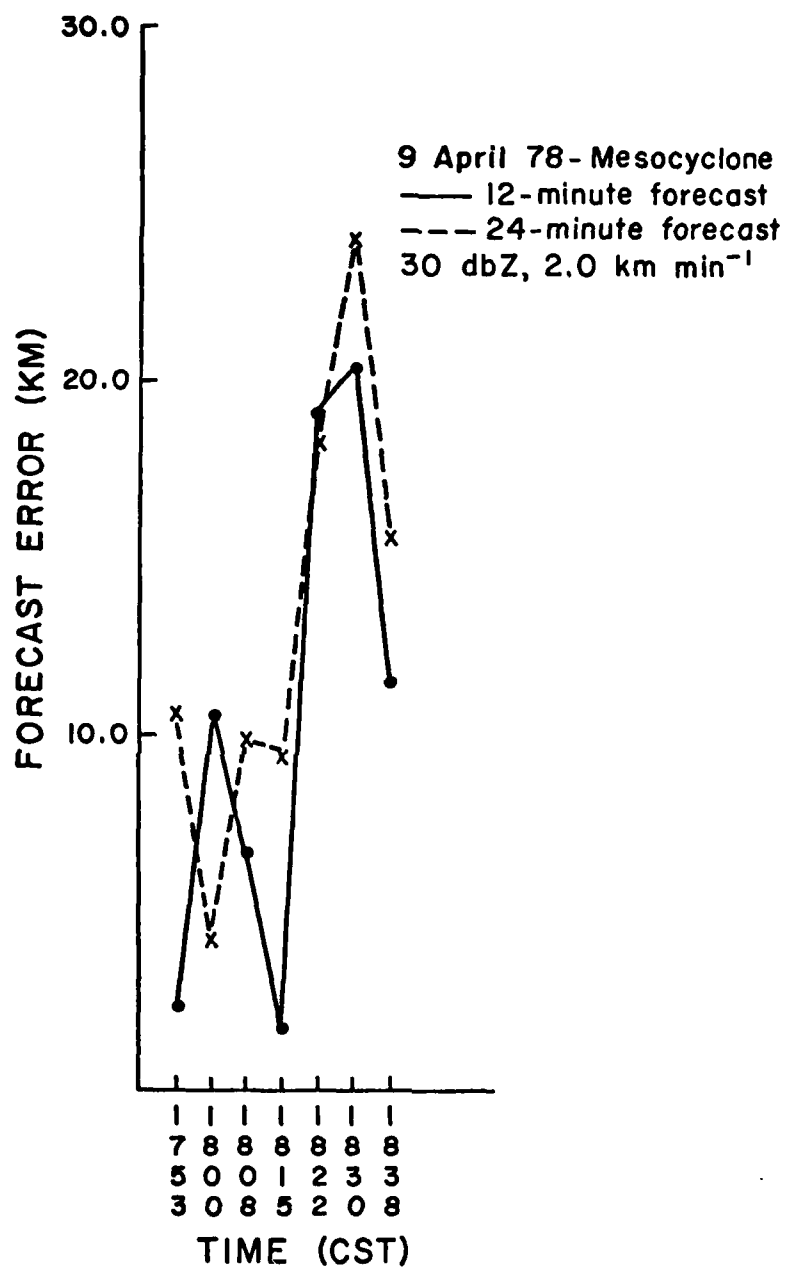
Fig. 25. Forecast errors for the 9 April
1978 storm producing the mesocyclone.
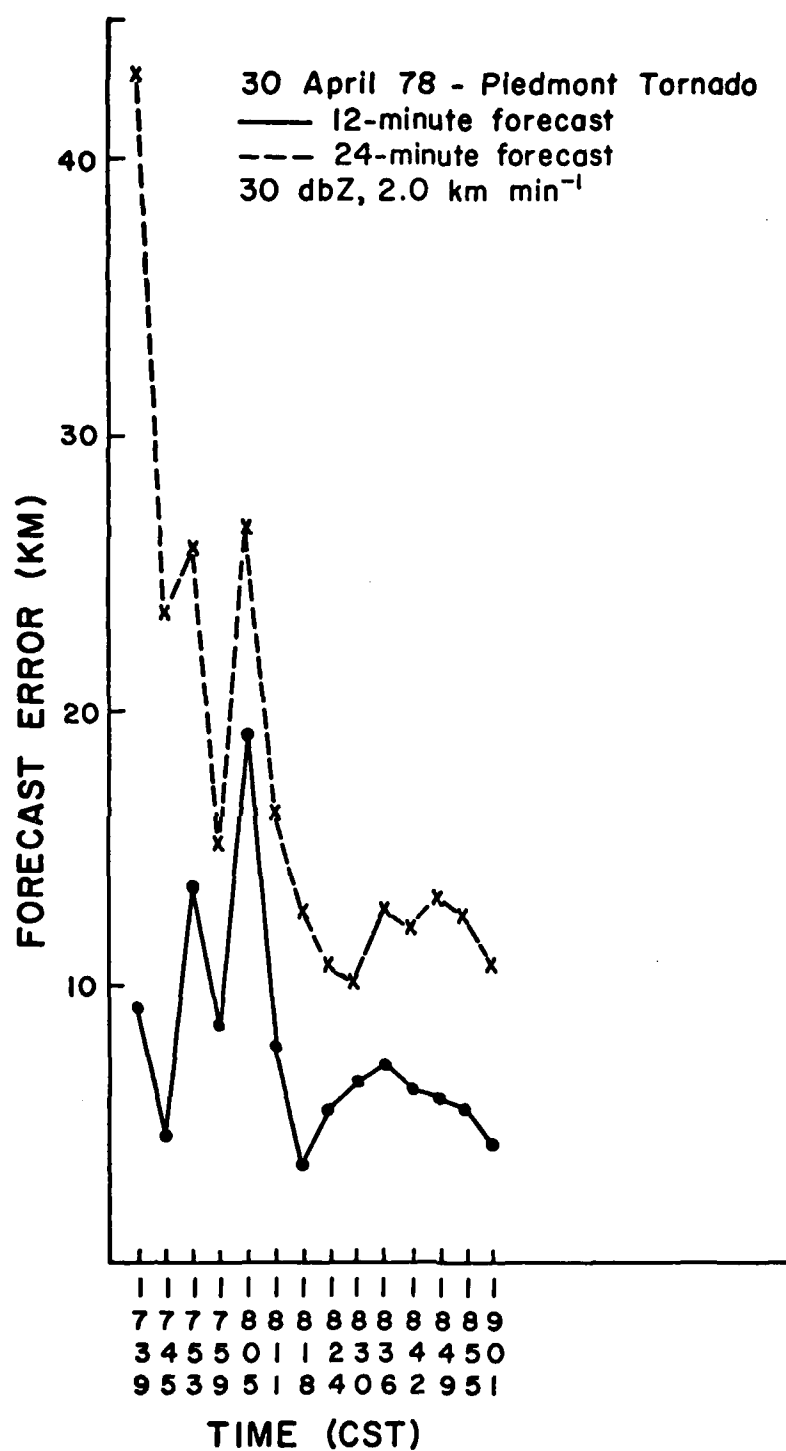
Fig. 26. Forecast errors for the 30 April 1978
storm producing the Piedmont tornado.
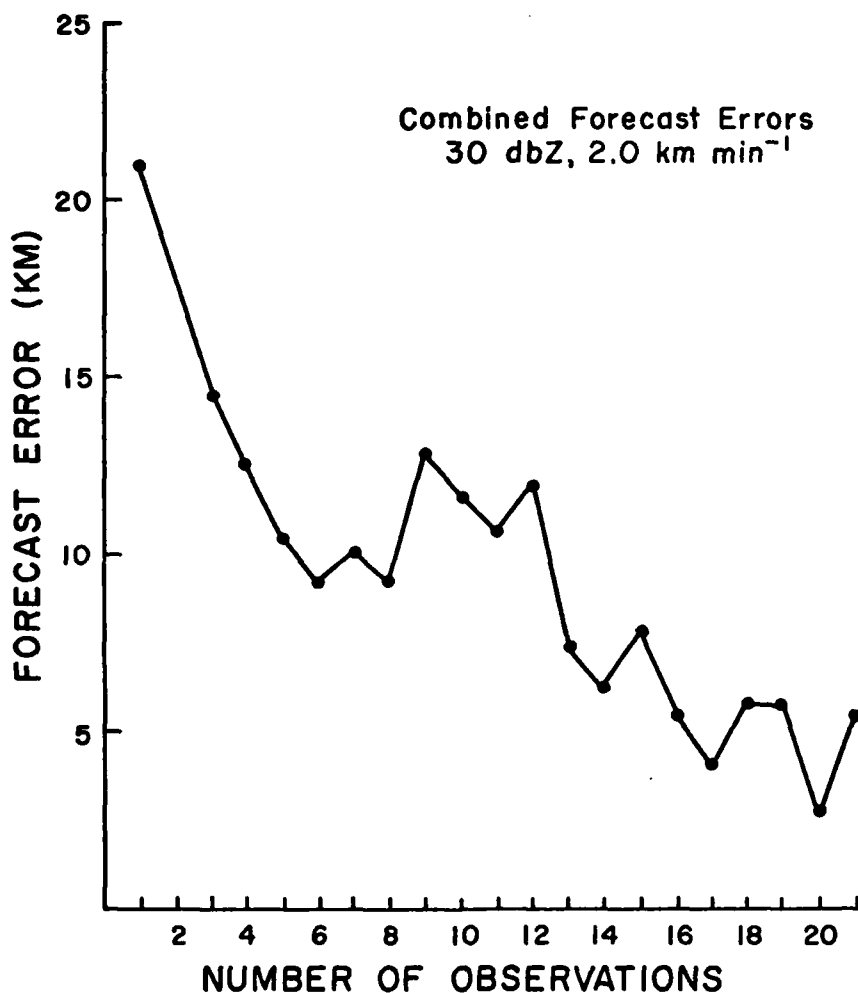
Fig. 27. Distribution of the forecast error with
number of observations used to make the forecast.
The forecast error is the average of all 12- and
24-min forecast errors whose forecast is based on
the same number of observations.

Table 1. National Severe Storms Laboratory Doppler Radar
Characteristics.

PARAMETER	NORMAN DOPPLER
Antenna	
Shape	Parabolic
Diameter	9.15 m
Half-Power Beam Width	0.81 deg.
Gain	46.8 db
First Side Lobe Level	21 db
Polarization	Vertical
RMS Surface Deviation	2.8 mm
Transmitter	
Wavelength	10.52 cm
Frequency	2850 MHz
Peak Power	750 kW
Pulse Width	1 μsec (150 m)

Table 2. Air Force Geophysics Laboratory Receiver Char-
acteristics.

PARAMETER	AFGL RECEIVER
Receiver	
System Noise Figure*	4 db
Transfer Function	Doppler - linear
	Intensity-Logarithmic
Dynamic Range	90 db
Minimum Detectable Signal	-105 db

*NSSL Doppler Radar

Table 3. Example of the correlation table. Table numbers are indices for finding other data corresponding to the related storms. Positive values indicate related storms, while negative values indicate non-related storms.

Storm \ Time	1	2	3	4	5	6	7	8............24
1	-1	2	1	0	0	0	0	0..............0
2	-2	-1	2	0	0	0	0	0..............0
3	-3	-3	-3	0	0	0	0	0..............0
4	-4	-4	-4	0	0	0	0	0..............0
5	-5	-5	-5	0	0	0	0	0..............0
6	-6	-6	-6	0	0	0	0	0..............0
7	-7	-7	-7	0	0	0	0	0..............0
8	-8	-8	-8	0	0	0	0	0..............0
9	-9	-9	-9	0	0	0	0	0..............0
10	-10	-10	-10	0	0	0	0	0..............0
11	-11	-11	-11	0	0	0	0	0..............0
12	-12	-12	-12	0	0	0	0	0..............0

Table 4. Severe activity on 5 April 1978 (Case 1).

TYPE	LOCATION (Oklahoma)	TIME (CST)
1-1½ in Hail	SW Major County to Cleo Springs	1800 – 1900
Tornado	Lone Wolf	1745 – 1755
High Winds Possible Tornado	NW Kingfisher to Southern Garfield County	1900 – 1930
Tornado	Pumkin Center	1955 – 2000
Wind Damage Golfball Hail	Stephens County	2000 – 2024
Tornado	Marlow	2024
Wind Damage	Garvin County, Pontotoc	2045 – 2200

Table 5. Severe activity on 9 April 1978 (Case 2).

TYPE	LOCATION (Oklahoma)	TIME (CST)
Wind Damage Hail	Kiowa County	1505 - 1605
High Winds	Caddo County	1648
Golfball Hail	Elk City	1420
Funnel Cloud	Alfalfa	1900
Wind Damage	Rocky Point	1730
1 in Hail	Hammon	1350
3/4 in Hail	Sayre	1356
Golfball Hail	Erick	1330
1 in Hail	Granite	1430
1 in Hail	Foss	1439

Table 6. Severe activity on 30 April 1978 (Case 3).

TYPE	LOCATION (Oklahoma)	TIME (CST)
Funnel Cloud	SW Grady County	1642
3/4 in Hail	W of Rush Springs	1700
1 in Hail	E of Rush Springs	1730
Tornado F0-F1	El Reno	1740
Tornado	E of El Reno	1750
Tornado	Richland	1755
Tornado	W of Richland to S Piedmont	1807 - 1815
Tornado	Piedmont to NW Oklahoma City and Edmond	1820 - 1835
Golfball Hail	SE Logan and N Lincoln Counties	2000 - 2100
Hail Wind Damage	E Logan, Lincoln and Pottawatomie Counties	2300
Tornado	Shattuck	1720
Wind Damage	Woodward	1955

Table 7. Results of sensitivity tests of reflectivity threshold (ZTH) and correlation radius (DCOR). Data includes the number of observations (N), mean forecast error ($\bar{X}_e$), and standard deviation (S) for Cases 1, 2, and 3 on 5 April 1978, 9 April 1978, and 30 April 1978, respectively.

| | CASE 1 – ZTH (dbz) | | | | | | | | | | | |
| | 1-25 | | | 1-30 | | | 1-35 | | | 1-40 | | |
DCOR (km min⁻¹)	N	$\bar{X}_e$	S	N	$\bar{X}_e$	S	N	$\bar{X}_e$	S	N	$\bar{X}_e$	S
1.0	8	10.47	7.19	6	9.03	7.07	–	–	–	–	–	–
1.2	27	5.40	5.33	10	13.38	9.40	4	6.88	4.38	–	–	–
1.4	48	7.23	6.38	31	8.60	7.03	18	7.89	5.46	–	–	–
1.6	98	7.23	5.88	68	10.01	10.53	36	8.79	7.75	–	–	–
1.8	131	9.28	7.88	123	9.12	7.95	56	8.47	7.04	7	13.80	7.24
2.0	154	10.58	9.44	141	9.96	7.77	95	9.16	7.30	14	15.59	7.48
2.2	159	10.67	9.37	164	9.86	7.40	111	8.36	6.32	14	15.59	7.48
2.4	162	10.79	9.40	174	10.34	7.87	117	8.80	6.46	14	15.59	7.48
2.6	187	12.52	9.79	181	10.93	8.51	119	9.08	6.83	14	15.59	7.48
2.8	182	13.55	10.49	188	11.12	8.26	128	9.55	7.37	14	15.59	7.48
3.0	193	15.23	11.98	187	12.47	10.49	128	9.55	7.37	14	15.59	7.48

Table 7. (Continued)

CASE 2 - ZTH (dbz)

DCOR (km min^{-1})	2-25			2-30			2-35			2-40		
	N	$\bar{X}_e$	S	N	$\bar{X}_e$	S	N	$\bar{X}_e$	S	N	$\bar{X}_e$	S
1.0	28	7.53	4.79	46	7.67	4.40	13	8.78	3.74	26	10.13	5.42
1.2	38	9.11	5.67	62	7.31	4.90	19	9.47	7.48	28	9.89	5.33
1.4	44	9.68	6.42	76	9.49	6.68	25	10.68	9.29	30	11.83	6.03
1.6	86	12.10	8.02	92	10.13	6.63	33	12.05	11.59	41	11.02	5.51
1.8	106	13.42	9.55	108	11.04	6.80	39	13.92	13.50	49	11.89	5.44
2.0	106	13.42	9.55	114	11.64	7.46	50	13.50	11.69	61	12.54	7.36
2.2	116	14.25	10.11	134	13.92	10.57	53	14.47	13.99	63	12.58	7.25
2.4	122	14.68	10.31	142	14.48	11.23	57	14.47	13.54	69	12.71	7.07
2.6	126	14.84	10.13	156	15.43	11.57	53	14.55	12.47	77	13.36	7.44
2.8	134	15.56	10.10	166	16.06	11.48	55	17.29	15.70	73	13.77	7.78
3.0	156	16.98	10.60	160	16.10	11.59	69	19.08	15.68	71	16.94	15.44

Table 7. (Continued)

CASE 3 - ZTH (dbZ)

DCOR (km min^{-1})	3-25			3-30			3-35			3-40		
	N	$\bar{X}_e$	s	N	$\bar{X}_e$	s	N	$\bar{X}_e$	s	N	$\bar{X}_e$	s
1.0	46	6.80	5.24	50	8.45	5.35	36	5.93	3.87	-	-	-
1.2	66	7.67	5.60	66	8.70	5.55	40	6.65	5.06	-	-	-
1.4	68	9.13	7.62	89	9.45	6.62	56	9.64	5.65	2	6.07	3.82
1.6	68	9.13	7.62	107	10.89	7.89	60	9.87	6.09	4	4.56	2.92
1.8	84	9.42	7.13	97	12.62	8.96	60	9.87	6.09	4	4.56	2.92
2.0	84	9.64	7.54	99	12.59	8.87	58	10.58	6.55	4	4.56	2.92
2.2	84	9.64	7.54	112	13.15	8.61	69	13.03	8.80	4	4.56	2.92
2.4	92	10.37	11.20	117	13.10	8.53	67	13.70	8.63	4	4.56	2.92
2.6	102	12.57	12.78	116	13.60	8.75	66	13.06	8.50	4	4.56	2.92
2.8	109	13.02	12.58	121	14.29	9.24	66	13.06	8.50	4	4.56	2.92
3.0	132	12.88	11.19	123	15.10	10.36	68	14.02	8.98	4	4.56	2.92

Table 8. Results of sensitivity tests for storm areas 4000 dbZ km^2 or greater. DCOR is 2.0 km min^{-1}. Abbreviations are the same as for Table 7.

CASE	ZTH (dbZ)	N (#)	$\bar{x}_e$ (km)	S (km)
1	25	95	8.01	5.56
	30	71	6.10	4.78
	35	14	8.01	7.03
	40	–	–	
2	25	76	12.04	8.46
	30	44	9.68	6.65
	35	19	10.90	7.80
	40	33	12.12	5.74
3	25	44	7.26	5.13
	30	40	14.19	10.13
	35	–	–	–
	40	–	–	–

Table 9. Array of individual mean forecast errors for the 12- and 24-min forecast. The 12- and 24-min combined value is indicated by Comb. ZTH is 30 dbZ and DCOR is 2.0 km min^{-1}. Abbreviations are the same as for Table 7.

CASE	FCST (min)	N (#)	$\bar{X}_e$ (km)	STANDARD DEVIATION (km)
1	12	70	7.45	5.63
	24	71	12.44	8.76
	Comb.	141	9.96	7.77
2	12	57	10.35	6.91
	24	57	12.94	7.83
	Comb.	114	11.64	7.46
3	12	50	8.53	5.44
	24	49	16.74	9.78
	Comb.	99	12.59	8.87

Table 10. Array of mean forecast errors for several individual storms. Abbreviations are the same as for Table 7.

CASE	STORM	FCST (min)	N (#)	$\bar{X}_e$ (km)	STANDARD DEVIATION (km)
1	Marlow Tornado	12	17	4.39	2.98
		24	18	6.42	3.03
		C	35	5.43	3.13
1	Southern Boundary	12	17	6.13	3.80
		24	18	12.47	6.61
		C	35	9.44	6.23
2	Heavy Rain	12	8	11.38	6.39
		24	8	12.60	8.41
		C	16	12.56	7.10
2	Mesocyclone	12	7	10.46	7.59
		24	7	13.37	6.52
		C	14	11.91	6.96
3	Piedmont Tornado	12	14	7.73	4.20
		24	14	17.66	9.33
		C	28	12.69	8.72

Table 11. Number of observations used to obtain forecast and mean forecast error.

# of Obs.	Sample Size	Mean Forecast Error (km)	Standard Deviation (km)
2	19	21.00	13.08
3	27	14.45	10.04
4	51	12.65	7.96
5	39	10.56	7.25
6	32	9.26	6.16
7	23	10.00	7.38
8	19	9.25	6.79
9	14	12.93	6.28
10	13	11.66	7.34
11	9	10.42	8.51
12	7	11.93	3.56
13	7	7.39	4.48
14	6	6.36	3.42
15	6	7.95	2.24
16	5	5.41	1.35
17	5	4.07	1.84
18	4	5.86	2.56
19	4	5.85	2.93
20	2	2.88	0.58
21	2	5.58	1.42